The Geological Society of America
Special Paper 542

Multiproxy Cretaceous-Paleogene boundary event stratigraphy: An Umbria-Marche basinwide perspective

Matthias Sinnesael
Department of Analytical, Environmental and Geo-Chemistry, Vrije Universiteit Brussel, Pleinlaan 2, B-1050 Brussels, Belgium

Alessandro Montanari
Osservatorio Geologico di Coldigioco, Contrada Coldigioco 4, 62021 Apiro, Italy

Fabrizio Frontalini
Rodolfo Coccioni
Dipartimento di Scienze Pure e Applicate, Università degli Studi di Urbino "Carlo Bo," Campus Scientifico, Località Crocicchia, 61029 Urbino, Italy

Jérôme Gattacceca
Centre National de la Recherche Scientifique, Aix-Marseille Université, Institut de Recherche pour le Développement (IRD), Coll France, National Institute for Agricultural Research (INRA), Centre de Recherche et d'Enseignement de Géosciences de l'Environnement (CEREGE), 13545 Aix-en-Provence, France

Christophe Snoeck
Department of Analytical, Environmental and Geo-Chemistry, Vrije Universiteit Brussel, Pleinlaan 2, B-1050 Brussels, Belgium

Wencke Wegner
Department of Lithospheric Research, University of Vienna, Althanstrasse 14, 1090 Vienna, Austria

Christian Koeberl
Department of Lithospheric Research, University of Vienna, Althanstrasse 14, 1090 Vienna, Austria, and *Natural History Museum, Burgring 7, 1010 Vienna, Austria*

Leah E. Morgan
U.S. Geological Survey, Denver Federal Center, MS 963, Denver, Colorado 80225, USA

Niels J. de Winter
Department of Analytical, Environmental and Geo-Chemistry, Vrije Universiteit Brussel, Pleinlaan 2, B-1050 Brussels, Belgium

Donald J. DePaolo
Earth Sciences Division, Lawrence Berkeley National Laboratory, Berkeley, California 94720, USA

Philippe Claeys
Department of Analytical, Environmental and Geo-Chemistry, Vrije Universiteit Brussel, Pleinlaan 2, B-1050 Brussels, Belgium

Sinnesael, M., Montanari, A., Frontalini, F., Coccioni, R., Gattacceca, J., Snoeck, C., Wegner, W., Koeberl, C., Morgan, L.E., de Winter, N.J., DePaolo, D.J., and Claeys, P., 2019, Multiproxy Cretaceous-Paleogene boundary event stratigraphy: An Umbria-Marche basinwide perspective, *in* Koeberl, C., and Bice, D.M., eds., 250 Million Years of Earth History in Central Italy: Celebrating 25 Years of the Geological Observatory of Coldigioco: Geological Society of America Special Paper 542, p. 133–158, https://doi.org/10.1130/2019.2542(07).

ABSTRACT

The complete and well-studied pelagic carbonate successions from the Umbria-Marche basin (Italy) permit the study of the event-rich stratigraphic interval around the Cretaceous-Paleogene boundary (e.g., Deccan volcanism, boundary impact, Paleocene recovery, and climate). To test the robustness of various proxy records (bulk carbonate $\delta^{13}C$, $\delta^{18}O$, $^{87}Sr/^{86}Sr$, and Ca, Fe, Sr, and Mn concentrations) inside the Umbria-Marche basin, several stratigraphically equivalent sections were investigated (Bottaccione Gorge, Contessa Highway, Fornaci East quarry, Frontale, Morello, and Petriccio core). Besides the classical Gubbio sections of Bottaccione and Contessa, the new Morello section is put forward as an alternative location for this stratigraphic interval because it is less altered by burial diagenesis. Elemental profiles (Ca, Fe, Sr, Mn) acquired by handheld X-ray fluorescence (pXRF) efficiently provide regional chemostratigraphic and paleoenvironmental information. The Deccan volcanism, the Cretaceous-Paleogene boundary, the characteristic pattern of the Sr/Ca profile across the boundary driven by the extinction and recovery of coccolithophores, and the Dan-C2 hyperthermal event are examples of such recorded paleoenvironmental events. Moreover, cyclostratigraphic analyses of proxies of detrital input (magnetic susceptibility and Fe concentrations) show the imprint in the sedimentary record of a 2.4 m.y. eccentricity minimum around 66.45–66.25 Ma, and suggest that the occurrence of the Dan-C2 hyperthermal event was astronomically paced.

INTRODUCTION

The Cretaceous-Paleogene boundary marks one of the major mass extinction events of the Phanerozoic (Raup and Sepkoski, 1982). The cause of the Cretaceous-Paleogene mass extinction is also one of the most debated ones (e.g., Schulte et al., 2010; comments by Archibald et al., 2010; Courtillot and Fluteau, 2010; Keller et al., 2010). Many Cretaceous-Paleogene boundary sections worldwide are characterized by the presence of iridium and other platinum group elements (PGEs), commonly in combination with ejecta layers that contain shocked minerals, spherules, and Ni-rich spinels (Alvarez et al., 1980; Smit and Hertogen, 1980; Montanari et al., 1983; Claeys et al., 2002; Schulte et al., 2010). Radioisotopic ($^{40}Ar/^{39}Ar$) dating of melt rock from the Chicxulub impact crater (Hildebrand et al., 1991; Swisher et al., 1992) and tektite-like glasses from several Cretaceous-Paleogene boundary sections (Renne et al., 2013) demonstrates their synchrony and supports the hypothesis that a large impact caused the mass extinction. An alternative hypothesis for the Cretaceous-Paleogene mass extinction is a causal relationship related to the emplacements of a large igneous volcanic province, the basaltic Deccan Traps (India). Radiometric dating of the Deccan basalts (^{40}K-^{40}Ar; Chenet et al., 2007; Renne et al., 2015) and other volcanic deposits (U-Pb; Schoene et al., 2015) shows that the second and main stage of Deccan volcanism started a few hundred thousand years before the Cretaceous-Paleogene boundary and lasted until at least the earliest Danian, including the Cretaceous-Paleogene extinction event. Additional arguments brought forward to support the Deccan volcanism hypothesis are based on other proxies that are interpreted as tracers for volcanic activity, such as: mercury (Hg) concentration and isotopic signatures, magnetic susceptibility properties, and the presence of the mineral akaganéite (Font et al., 2011, 2016; Sial et al., 2016; Font et al., 2018; Keller et al., 2018). The stratigraphic interpretation of records used in these studies is, however, subject to debate (e.g., Smit et al., 2016; Mukhopadhyay et al., 2017), as well as the variable impact of different volcanogenic processes on the efficiency of Hg dispersal across the globe (Percival et al., 2018). Recently, a new hypothesis was presented, which suggests that the impact itself triggered a major increase in the activity of Deccan volcanism (Renne et al., 2015; Richards et al., 2015) and global magmatism, such as, for example, at mid-ocean ridges (e.g., Byrnes and Karlstrom, 2018).

Complete and well-studied sedimentary successions, like the marine pelagic carbonates from the Umbria-Marche basin (Italy), are suitable archives that can help to dissect this event-rich stratigraphic interval. The Cretaceous-Paleogene boundary was biostratigraphically defined for the first time in the classical sections of Gubbio, one of the Cretaceous-Paleogene boundary sections in the Umbria-Marche basin (Luterbacher and Premoli Silva, 1964). Moreover, in these Gubbio sections Alvarez et al. (1980) first reported the presence of an iridium anomaly that led to the hypothesis of an asteroid impact causing the Cretaceous-Paleogene mass extinction. Besides the Cretaceous-Paleogene boundary event itself, the continuous and complete sedimentary records in Gubbio provide the opportunity to investigate the signatures of other events preceding and following the Cretaceous-Paleogene boundary event (e.g., Coccioni et al., 2012, 2013). A decline in the marine osmium isotopic ($^{187}Os/^{188}Os$) record a few hundred thousand years before the Cretaceous-Paleogene

boundary was interpreted as a chemostratigraphic marker for the beginning of the second and main phase of Deccan volcanism (Ravizza and Peucker-Ehrenbrink, 2003) and was also identified in the Bottaccione Gorge section at Gubbio (Robinson et al., 2009). The mass extinction itself was followed by an ecological recovery (e.g., D'Hondt et al., 1998; Coxall et al., 2006; Coccioni et al., 2010; Schulte et al., 2010). A typical feature of the post–Cretaceous-Paleogene boundary event climatic system of the Paleogene is the occurrence of numerous hyperthermal events, with the Paleocene-Eocene thermal maximum being the most prominent example (Kennett and Stott, 1991; Zachos et al., 2001). The exact mechanism(s) behind these hyperthermals is still debated (e.g., Dickens et al., 1995; Sluijs et al., 2007; Zeebe et al., 2009), but the timing appears to be astronomically paced (Lourens et al., 2005; Galeotti et al., 2010; Littler et al., 2014; Lauretano et al., 2015; Laurin et al., 2016). The Dan-C2 is the first of these Paleogene hyperthermal events (Quillévéré et al., 2008), and it was identified just above the Cretaceous-Paleogene boundary at Gubbio by Coccioni et al. (2010).

It is common practice to compare different chronologically equivalent records from various geographic locations and sedimentary settings. This is necessary to assess the potential global nature and variability of worldwide climatic events such as the Cretaceous-Paleogene event. In this study, the robustness of proxy records inside the same basin (i.e., Umbria-Marche) is tested for the stratigraphic interval encompassing the Cretaceous-Paleogene boundary by investigating various stratigraphically equivalent sections of Gubbio, including the new Morello section. The Gubbio sections encompassing the Cretaceous-Paleogene boundary were recently investigated in detail using an integrated multiproxy cyclostratigraphic approach focusing on sedimentology and temporal framework (Sinnesael et al., 2016a, 2018). The application of portable X-ray fluorescence (pXRF) for chemostratigraphic correlations with other locations in the same basin (using Fe, Ca, Sr and Mn profiles) was tested. To verify these pXRF correlations with the well-established Gubbio stratigraphy, classical stratigraphic tools, such as biostratigraphy and magnetostratigraphy, and $\delta^{13}C$ and $^{87}Sr/^{86}Sr$ isotope chemostratigraphy, were applied on the continuous Cretaceous-Paleogene boundary section at Morello. The new Cretaceous-Paleogene section at Morello is stratigraphically complete, easily accessible, seems less affected by burial diagenesis than Gubbio, and offers a good alternative for further studies next to the heavily sampled Gubbio sections. The new data from Gubbio and stratigraphically equivalent sections allow the reconstruction of more robust patterns in this events-rich interval encompassing the Cretaceous-Paleogene boundary.

GEOLOGICAL AND STRATIGRAPHIC SETTING

The classical sections at Gubbio (Bottaccione [BOT] and Contessa [COH]; Fig. 1B) are known for pioneering work on the Cretaceous-Paleogene boundary interval (Luterbacher and Premoli Silva, 1964; Alvarez et al., 1977, 1980). These sections are part of the larger Umbria-Marche basin succession of pelagic carbonates continuously spanning the Lower Jurassic to the Upper Miocene. The Maastrichtian R2 member of the Scaglia Rossa Formation (Montanari et al., 1989) is characterized by pink biomicritic limestone made up of planktonic foraminiferal tests suspended in a coccolith matrix with a terrigenous component of silt and clay considered to be of eolian origin (Arthur and Fischer, 1977; Johnsson and Reynolds, 1986; Sinnesael et al., 2016a). The Danian R3 member is also part of the Scaglia Rossa Formation but contains more marly intervals interbedded with pelagic limestones as compared to the Maastrichtian R2 member (Montanari et al., 1989). The Umbria-Marche basin contains multiple other Cretaceous-Paleogene boundary sections, from which the following were investigated in this study (Fig. 1): Fornaci East quarry (FOE), Frontale (FRO), Morello (MRL), and the Petriccio core (PTC).

MATERIALS AND METHODS

Planktonic Foraminiferal Biostratigraphy at the Morello Section

The biostratigraphic study of the MRL section (Fig. 2A) focused on a 16-m-thick stratigraphic segment across the Cretaceous-Paleogene boundary and analyzed 29 samples collected from the upper 12 m section of the Maastrichtian (average resolution of ~0.41 m) and 27 samples in the lower 4 m section of the Danian (average resolution of ~0.15 m). Samples were treated following the cold acetolysis technique of Lirer (2000) by sieving through a 42 µm mesh and drying at 50 °C. This method enabled the extraction of generally easily identifiable foraminifera even from indurated limestones, providing the possibility for accurate taxonomic determination and detailed analysis of foraminiferal specimens. All the studied materials are housed in the laboratory of the Dipartimento di Scienze Pure e Applicate, Università di Urbino, Urbino, Italy. The planktonic foraminiferal standard zonations of Coccioni and Premoli Silva (2015) for the Cretaceous and of Wade et al. (2011) for the Paleogene were followed.

Magnetostratigraphy at Morello Section

Oriented core samples were obtained from 19 levels between –9.00 m and +2.20 m in the MRL section (Fig. 2A). In this study, negative meter levels will consequently represent Maastrichtian strata, and positive meter levels represent Danian strata. They were drilled using an electric corer with a 25-mm-diameter diamond bit barrel. Samples were then segmented with a diamond disk saw at the Geological Observatory of Coldigioco (Italy) to obtain standard cylindrical paleomagnetic samples (i.e., 25-mm-diameter, 22-mm-height samples) from each level. Natural remanent magnetization (NRM) was measured at the Centre Européen de Recherche et d'Enseignement des Géosciences de l'Environnement (CEREGE, Aix-en-Provence, France) using a SQUID magnetometer (model 755R from 2G Enterprises) with a noise level of 10^{-11} Am^2.

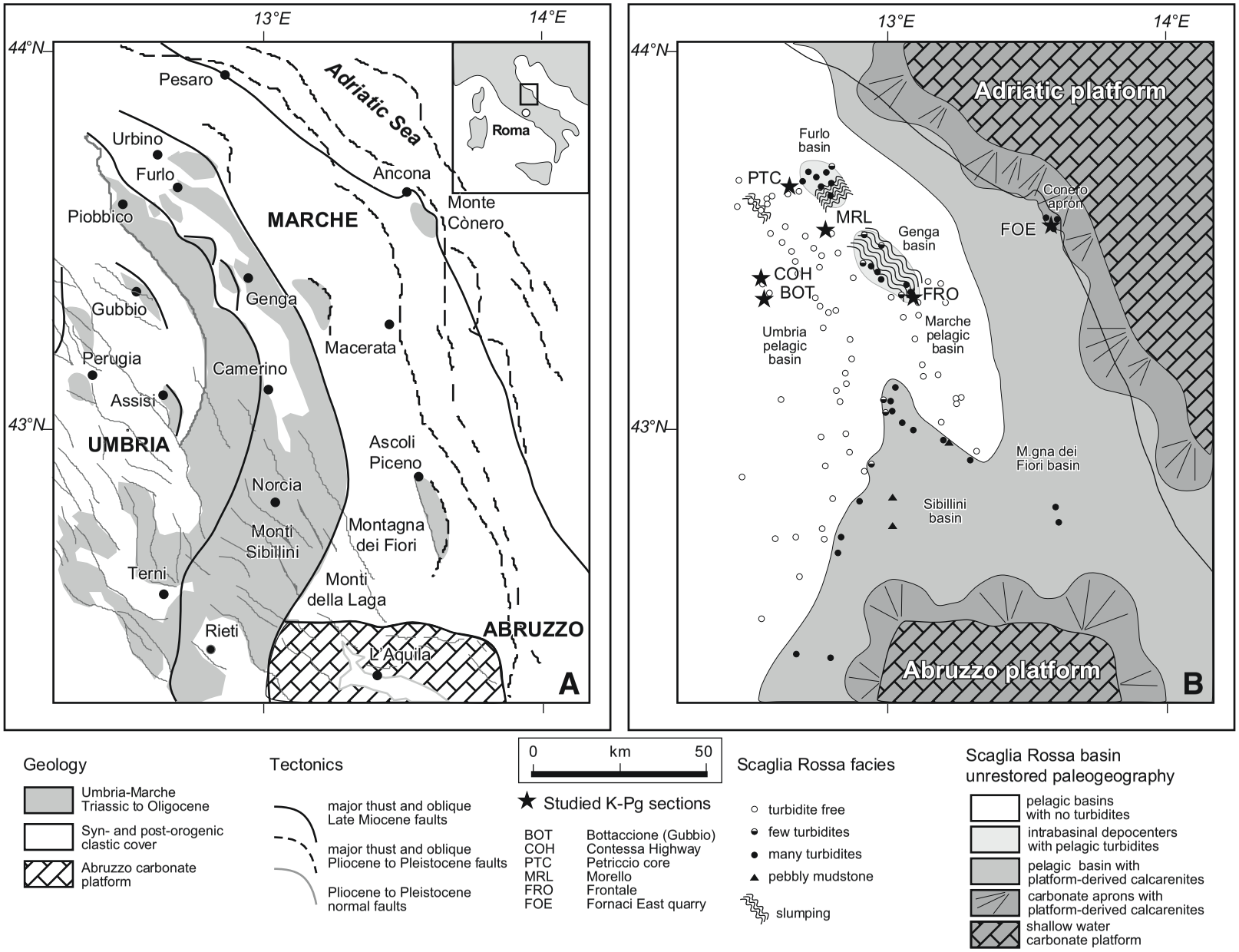

Figure 1. (A) Simplified geological and structural map of the Umbria-Marche basin, Italy. (B) Late Cretaceous paleogeographic reconstruction of the Umbria-Marche basin (adapted from Bice et al., 2007). Locations of the studied stratigraphic sections: BOT—Bottaccione Gorge section (43°21′58.0″N, 12°34′57.5″E); COH—Contessa Highway section (43°21′46.9″N, 12°33′44.1″E); FOE—Fornaci East quarry (43°33′12.72″N, 13°35′12.8″E); FRO—Frontale (43°20′58.6″N, 13°05′48.8″E); MRL—Morello (43°29′50.5″N, 12°48′38.2″E); PTC—Petriccio core (43°36′41.9″N, 12°38′44.2″E). K-Pg—Cretaceous-Paleogene.

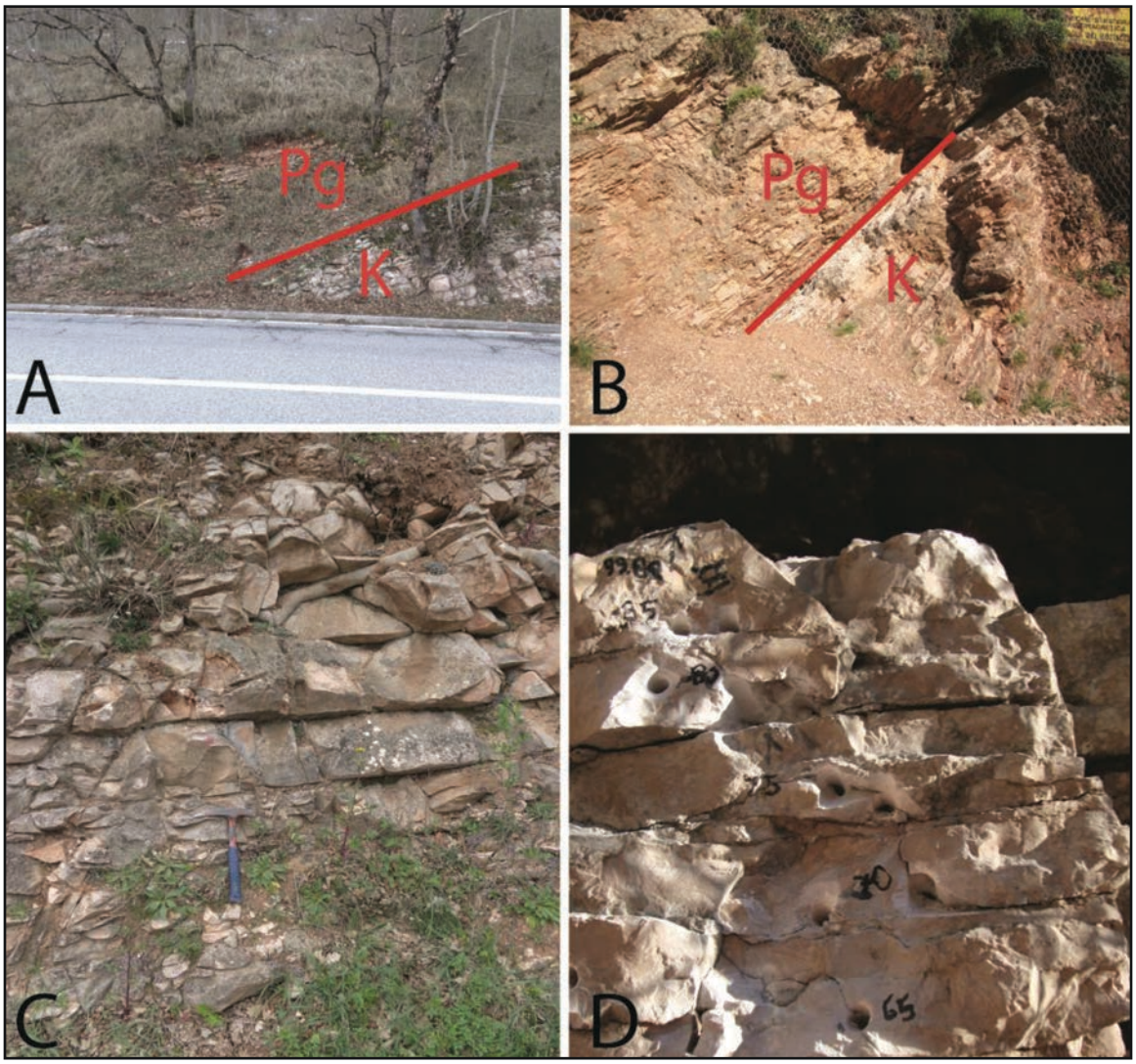

Figure 2. (A) Overview picture of the Morello section. (B) Overview picture of the Bottaccione section. (C) Detail of the Maastrichtian bedding in Morello showing the 30–40-cm-thick bedding (hammer for scale). (D) Detail of the Maastrichtian bedding in Bottaccione showing stylolitization and less clear bedding compared to Morello (for scale: numbers are in cm). K-Pg—Cretaceous-Paleogene.

Samples were demagnetized using alternating fields (AF). Demagnetization data were evaluated using principal component analyses (Kirschvink, 1980). All paleomagnetic data were processed using PaleoMac software (Cogné, 2003).

Samples for Bulk Geochemistry

Bulk sampling for geochemical analyses targeted the pink biomicritic limestone, which is made up of planktonic foraminiferal tests suspended in a coccolith matrix. Samples from the upper 7.2 m of the Maastrichtian in BOT were sampled by Sinnesael et al. (2016a) at regular 5.0 cm intervals (~40 g powder) using an electric drill (Fig. 2D). The meter levels used in Sinnesael et al. (2016a) were rescaled such that the Cretaceous-Paleogene boundary is at the 0 m level in this work, instead of 100 m level. The lowest 4.0 m section of the Danian in COH was sampled at regular 2.5 cm intervals by collecting small hand samples (~30 cm^3) with hammer and chisel from the cleaned outcrop. At MRL (Fig. 2C), similar hand samples were taken from the upper 6.0 m of the Maastrichtian (every 5.0 cm) and lower 2.5 m of the Danian (every 2.5 cm). At FOE, hand samples were taken from the upper 4.7 m of the Maastrichtian (every 5.0 cm) and lower 0.6 m of the Danian (every 2.5 cm). Analyses of the FRO section with pXRF were done on a single polished slab spanning the upper 0.6 m of the Maastrichtian (every 15.0 cm) and lower 0.15 m of the Danian (every 2.5 cm). The pXRF analyses on the

PTC core spanned the upper 1.25 m of the Maastrichtian (every 5.0 cm) and lower 1.80 m of the Danian (every 2.5 cm) after cleaning and polishing the core surface. Sampling was done at a higher resolution for the Danian than the Maastrichtian because of the lower sedimentation rate of the Danian strata (e.g., Mukhopadhyay et al., 2001; Sinnesael et al., 2016a).

A larger hand sample was acquired from −1.50 m in the BOT section to study the geochemical signature ($\delta^{13}C$, $\delta^{18}O$, and concentrations of Ti, K, Fe, Ca, and Sr) of calcite veins and stylolites (pressure solution surfaces) at a high spatial resolution (Sinnesael et al., 2018). Six samples were drilled for isotopic analyses ($\delta^{13}C$, $\delta^{18}O$) with varying compositions. The first type of composition contains pure calcite from a calcite vein, a second is mixed calcite vein with surrounding pink matrix, the third type is mixed stylolite with surrounding matrix, and the fourth type contained a pure pink micritic matrix.

X-Ray Fluorescence Measurements

Portable X-ray fluorescence measurements were carried out on polished surfaces of hand or core samples using a Bruker Tracer IV handheld portable XRF device (HHpXRF, hereafter pXRF) equipped with a 2 W Rh anode X-ray tube and a 10 mm^2 silicon drift detector (SDD) with a resolution of 145 eV (Mn-Ka). All pXRF measurements were carried out by placing the pXRF nozzle directly on the flat sample surface. All analyses were carried out in duplicate with a measurement time of 30 s, and concentrations reported in this study are averages of both measurements. This integration time was sufficient for the time of stable reproducibility (TSR) and the time of stable accuracy (TSA) to be reached for individual point spectra for all elements considered in this study (see de Winter et al., 2017a). Further technical details on the pXRF measurements and calibration can be found in Sinnesael et al. (2018). The results of the pXRF measurements carried out for Ca, Mn, Fe, and Sr are available in the Supplementary Materials (Table DR1).[1]

Micro-XRF mapping and line scans were carried out at the Vrije Universiteit Brussel (VUB), Brussels, Belgium, using the Bruker M4 Tornado micro-XRF (hereafter: μXRF). Technical details on the μXRF measurements may be found in de Winter and Claeys (2017). These conditions allowed concentrations of major and trace elements to be characterized only semiquantitatively for the mapping (see de Winter et al., 2017b).

Stable Isotopes ($\delta^{13}C$ and $\delta^{18}O$)

Measurements of carbon ($\delta^{13}C$) and oxygen ($\delta^{18}O$) stable isotope ratios of the bulk carbonate rock were carried out at the VUB, using a Nu Perspective isotope ratio mass spectrometer (IRMS; Nu Instruments, UK) interfaced with a Nu Carb automated carbonate device. Acidification of the samples occurred at a temperature of 70 °C. All values are expressed relative to the Vienna Peedee belemnite (‰, VPDB) standard. Calibration was carried out using an in-house Marbella limestone (MAR) standard (+3.41‰ VPDB, –0.13‰ VPDB) calibrated against the international NBS-19 standard. On the basis of replicated measurements of the MAR standard, reproducibility errors on $\delta^{13}C$ and $\delta^{18}O$ were determined to be <0.05‰ (1σ) and <0.10‰ (1σ), respectively. Corrected $\delta^{13}C$ and $\delta^{18}O$ carbonate stable isotope ratios are available in Table DR2 (see footnote 1).

Strontium Isotopes ($^{87}Sr/^{86}Sr$)

This study integrated various published and previously unpublished $^{87}Sr/^{86}Sr$ data sets from different sections from the Umbria-Marche basin. The Sr isotope ($^{87}Sr/^{86}Sr$) results from the Maastrichtian strata of BOT (N = 12) were published in Sinnesael et al. (2018). The exact same analysis technique, analyzing the whole rock and carbonate fraction with multicollector–inductively coupled plasma–mass spectrometry (MC-ICP-MS) at the GTime laboratory of the Université Libre de Bruxelles, Belgium, was used in this study to analyze the Danian COH (N = 23) and the lowermost Danian and upper Maastrichtian MRL (N = 12) samples. These measurements have uncertainties (2σ) of 0.000040 (N = 15 on the NBS-987 standard). Additionally, 32 whole-rock limestone samples (and four samples only containing the carbonate fraction) from the MRL section were selected for Sr thermal ionization mass spectrometry (TIMS) isotope analysis. The TIMS Sr isotope measurements were performed at the Laboratory of Geochronology, Department of Lithospheric Research, University of Vienna, Austria. Before chemical treatment, weathering crusts were removed mechanically, and samples were crushed in a disc mill to make homogenous powders (<63 μm) from which ~50 mg aliquots were used for analysis. Sample dissolution was performed using 6 N HCl (or 0.1 N CH_3COOH for a test sequence), and element separation followed conventional procedures, using AG® 50 W- X8 (200–400 mesh, Bio-Rad) resin and 2.5 N HCl as elution medium. Total procedural blanks for Sr were <1 ng. Sr fractions were loaded as chlorides and evaporated from a Re double filament, using a Thermo Finnigan® Triton TI TIMS. An $^{87}Sr/^{86}Sr$ ratio of 0.710252 ± 0.000002 (N = 7) was determined for the NBS-987 (Sr) international standard during the period of investigation. Within-run mass fractionation was corrected for $^{86}Sr/^{88}Sr$ = 0.1194. Uncertainties on the Sr isotope ratios are quoted as 2σ.

These recent $^{87}Sr/^{86}Sr$ results were integrated with a previously unpublished data set from the early nineties, which were collected by some of the coauthors and analyzed at the Berkeley Center for Isotope Geochemistry. In total, these data originated from various locations in the Umbria-Marche basin and spanned a larger stratigraphic interval (Campanian up to Ypresian) than just the Cretaceous-Paleogene boundary interval. Most of the

[1]GSA Data Repository Item 2019216—Table DR1: pXRF; Table DR2: Stable isotopes; Table DR3: Strontium isotopes; Table DR4: $^{40}Ar/^{39}Ar$_ALE_dating (USGS Data Release: https://doi.org/10.5066/P9WOEI1N)—is available at www.geosociety.org/datarepository/2019/, or on request from editing@geosociety.org or Documents Secretary, GSA, P.O. Box 9140, Boulder, CO 80301-9140, USA.

data were taken from BOT and COH on the bulk carbonate fraction. The samples were washed in extremely dilute acetic acid prior to dissolution using 3 mL of distilled water and 20 µL of subboiled glacial acetic acid ultrasonically agitated for 30 min, following the method outlined by McArthur et al. (1993). The treatment is expected to preferentially dissolve cements and overgrowths and leach radiogenic Sr present on exchangeable sites on clays. About 15% of the sample was dissolved in this first wash solution. The washed samples were centrifuged, the supernatant was discarded, and the residue was leached in an identical acidic solution for another 30 min. After subsequent centrifugation, the solution was evaporated to dryness. The impure $CaCO_3$ thus obtained was redissolved in 1.5 *N* HCl, and the Sr fraction was collected after passing the solution through ion exchange columns. This was again evaporated to dryness. Approximately 10 ng amounts of the Sr from each sample were loaded onto a Re filament with Ta oxide for analysis in a VG Sector 354 MC-ICP-MS in dynamic multicollection mode. Two standards of NBS-987 and two of modern seawater (MS) were run in each turret of 20 samples. Column blanks averaged 183 ± 97 pg Sr, which is negligible for carbonate samples.

It is possible that secondary cements have $^{87}Sr/^{86}Sr$ ratios different from that of the original microfossils, so that the overall acid soluble fraction contains diagenetically redistributed Sr. To enable some evaluation of diagenetic effects, we analyzed several samples of inoceramid bivalves found articulated and presumably in life position in the limestone, as well as fish teeth extracted from the marl layers. Both the phosphate and low-Mg calcite in these samples may be diagenetically modified to some degree, but the magnitude of the Sr isotopic difference between these samples and the bulk carbonate samples gives some indication of the severity of diagenetic modification. All $^{87}Sr/^{86}Sr$ data with respective sample sections, stratigraphic levels, and measuring techniques are available in the Table DR3 (see footnote 1).

$^{40}Ar/^{39}Ar$ Dating ALE Volcanic Ash

Samples from the volcanic ash "Livello Alessandro" (ALE; Odin et al., 1992) were collected both from COH (at stratigraphic level 2.00 m) and MRL (at stratigraphic level 2.45 m). Biotite grains were handpicked after wet sieving using the >63 µm fraction. Unfortunately, the biotite grains from the MRL-ALE sample were too small to date accurately, so only the COH-ALE data are presented in this study. The $^{40}Ar/^{39}Ar$ analytical methods were largely as described in Kavalieris et al. (2017), with variations noted here. Samples were irradiated for 20 h. Background measurements were run every three analyses; backgrounds were fit with a mean ± standard deviation. Discrimination and detector intercalibration factors were determined via measurements of three air pipettes approximately twice per day. The sample was co-irradiated with Fish Canyon sanidine (FCs), and ages were calculated using ^{40}K decay constants and an age for FCs of 28.294 ± 0.036 Ma (1σ) from Renne et al. (2011), so that results can be compared directly to the Cretaceous-Paleogene age from Renne et al. (2013). For reference, ages for each analyzed grain were also calculated using other possible FCs age and decay constant combinations. See the full raw data table provided in Table DR4 (see footnote 1).

Time-Series Analysis

Cyclostratigraphic analyses were carried out using sliding fast Fourier transformations (FFT) in Matlab®. The algorithms were modified from Muller and MacDonald (2000) and were explained in detail by Bice et al. (2012). The data were linearly detrended and padded with zeros prior to analysis. This approach has been successfully applied in other cyclostratigraphic studies in the Umbria-Marche basin (e.g., Cleaveland et al., 2002; Sinnesael et al., 2016a; Montanari et al., 2017). The MRL Fe concentrations (pXRF) data were used for the Maastrichtian (5 cm resolution and window size of 2 m), and the COH magnetic susceptibility data from Sinnesael et al. (2016a) were used for the Danian (1 cm resolution and window size of 0.7 m). This is a composite record using two different proxies from two different sections. The motivation for this selection was to use the respective best-quality records with the highest available stratigraphic resolution. Cyclostratigraphic analyses of magnetic susceptibility and pXRF Fe data on sediments from the Scaglia Rossa Formation have been shown to be basically interchangeable (Sinnesael et al., 2018).

RESULTS

Planktonic Foraminiferal Biostratigraphy at the Morello Section

Planktonic foraminifera are continuously present and abundant throughout the study interval, with diverse genera and species typical of late Maastrichtian–early Danian low-latitude pelagic environments. Preservation varies from poor to good, but it is mostly moderate to good and therefore offers the possibility for accurate taxonomic determinations and detailed analysis of foraminiferal assemblages (not presented here). All the marker species that define the standard planktonic foraminiferal zones of Coccioni and Premoli Silva (2015) for the Cretaceous and of Wade et al. (2011) for the Paleogene occurred in the analyzed material. The common planktonic foraminiferal biozones for this stratigraphic interval were identified, and the locations of the boundaries are reported in Table 1.

Paleomagnetic Results at the Morello Section

The AF demagnetization was efficient to reveal the characteristic remnant magnetization (ChRM) after removal of an overprint up to ~20 mT (Fig. 3). After tilt correction, there is clear dichotomy between samples up to −3.05 m (normal polarity ChRM; Fig. 3A) and above −2.95 m (reverse polarity ChRM; Fig. 3B). The normal and reverse direction populations

TABLE 1. STRATIGRAPHIC LEVELS OF BIOSTRATIGRAPHIC, MAGNETOSTRATIGRAPHIC, AND CHEMOSTRATIGRAPHIC EVENTS ACROSS THE CRETACEOUS-PALEOGENE BOUNDARY IN THE BOTTACCIONE-CONTESSA HIGHWAY (BOT-COH) COMPOSITE SECTION COMPARED TO THE MORELLO SECTION

Boundaries and events	Morello (m)	Gubbio (BOT-COH) (m)
P1a-P1b	2.60	2.25
"Livello Alessandro" (ALE) volcanic ash	2.45	2.00
C29r-C29n upper potential boundary	1.75	1.20
C29r-C29n lower potential boundary	1.42	1.20
Dan-C2 hyperthermal peak dissolution	0.95	0.80
$\delta^{13}C$ 'drop'	0.70	0.60
P0/Pα-P1a	0.70	0.55
Cretaceous-Paleogene (K-Pg) boundary	0.00	0.00
Plummerita hantkeninoides–Pseudotextularia elegans	–1.50	–1.41
Local $\delta^{13}C$ minimum	–1.95	–1.65
Local $\delta^{13}C$ maximum, also knickpoint in Mn profile	–3.55	–3.15
C30n-C29r upper potential boundary	–3.70	–3.80
C30n-C29r lower potential boundary	–4.10	–3.80
Pseudotextularia elegans–Pseudoguembelina hariaensis	–5.50	–4.83

yielded a positive reversal test (McFadden and McElhinny, 1990), strongly suggesting that the ChRM is a primary magnetization (Fig. 4). For two of the reverse polarity samples (level –2.00 m and –0.20 m), the ChRM direction could not be defined with enough precision because of spurious demagnetization behavior at high AF. One of the normal polarity samples (level –8.80 m) had a slightly deviating direction and may have been misoriented in the field. These analyses indicate that the magnetostratigraphic boundary in the MRL section between chrons C30n and C29r is placed between levels –4.10 m and –3.70 m, and the C29r-C29n boundary is between 1.42 m and 1.75 m (Table 1).

Portable XRF Measurements

The Gubbio Ca profile oscillates around 35 wt% for the Maastrichtian strata in the BOT section and decreases across the Cretaceous-Paleogene boundary toward lower values around 30 wt% for the COH Danian strata (Fig. 5). The boundary clay layer is clearly visible in the profile as the minimum at the 0.00 m level (Fig. 5). The ALE volcanic ash is also clearly marked by a local minimum at the 2.00 m level. The Fe profile displays the opposite trends as the Ca profile, as both are respectively proxies for the clay (detrital) versus calcium carbonate content. The main feature of the Gubbio Sr profile is a sharp decrease

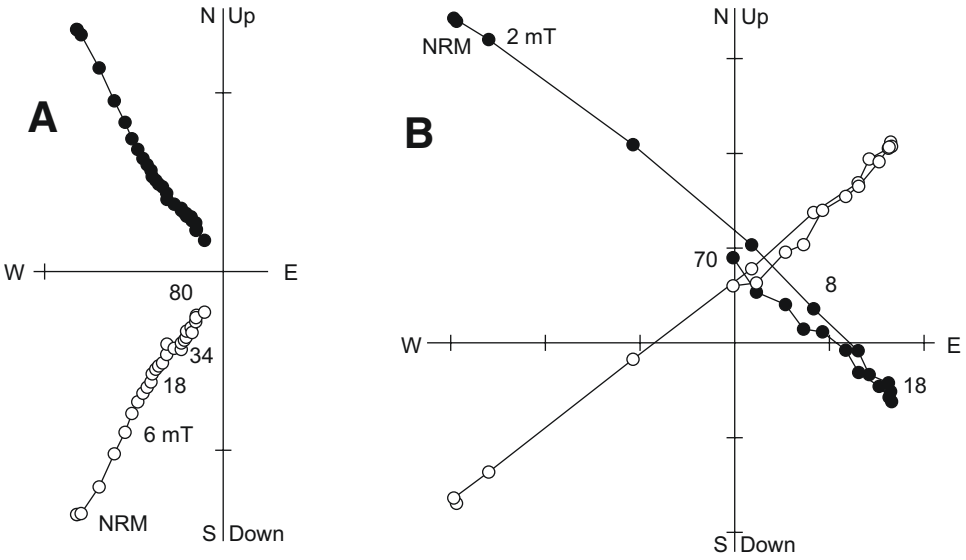

Figure 3. Orthogonal projection plots of stepwise alternating field (AF) demagnetization data of representative normal (level 92.00 m = –8.00 m) and reverse (level 97.05 m = –2.95 m) polarity samples. Open and solid symbols represent projections on the horizontal and vertical plane, respectively. NRM—natural remanent magnetization.

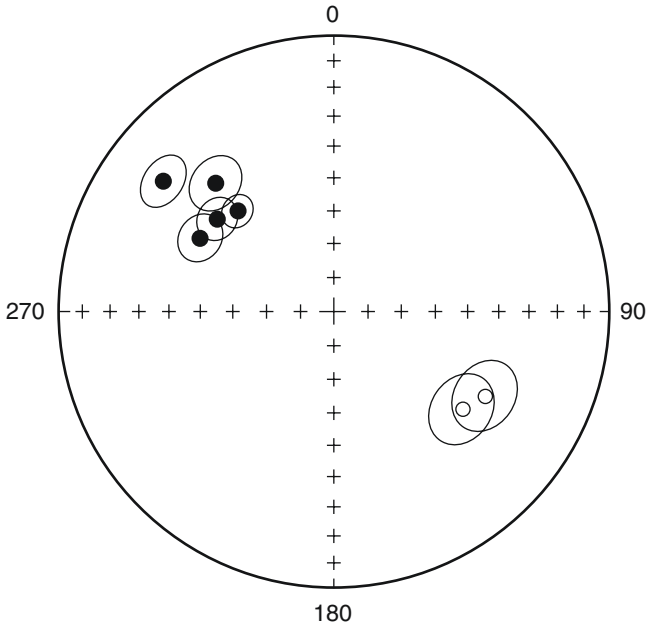

Figure 4. Stereographic projection of the characteristic remanent magnetization (ChRM) directions of the seven samples for which a well-defined ChRM could be defined (except outlying direction from level 91.20 m). The maximum deviation angle (MAD; Kirschvink, 1980) of each direction is shown.

across the Cretaceous-Paleogene boundary from Maastrichtian concentrations of 700–800 ppm (with several enrichments up to 1000 ppm in the upper half of the Maastrichtian) to 200–300 ppm right after the boundary (Fig. 5). Danian Sr concentrations seem to rise steadily, except for a small increase to values of 500–600 ppm between 0.25 and 0.35 m. The variability in the Sr concentration signal increases in the upper half meter (3.50–4.00 m). The Gubbio Mn profile for the Maastrichtian is relatively stable with values of 300–400 ppm and shows a sudden increase of 200 ppm after the Cretaceous-Paleogene boundary (Fig. 5). The Mn concentration decreases toward the 3.00 m level, after which it slowly increases again. Elevated Mn concentrations are also found in the ALE volcanic ash.

The Ca, Fe, Sr, and Mn profiles for the MRL section show the same trends as the Gubbio elemental profiles (Figs. 5 and 6). The decrease in Ca and corresponding increase in Fe are more pronounced for the MRL data series. There is also a larger difference in amplitude variability for the MRL Ca and Fe data compared to the Gubbio profiles (Figs. 5 and 6). The Cretaceous-Paleogene boundary clay itself and the MRL-ALE level (2.45 m) were not sampled and measured in MRL, and therefore both sedimentological features are not visible in the respective profiles. There is a clear local maximum in the MRL Fe profile (Ca minimum) at level 0.95 m (Fig. 6), which is also present in Gubbio at level 0.80 m (Fig. 5). In contrast to the Maastrichtian Sr profile in Gubbio (Fig. 5), the Maastrichtian MRL profile does not show enrichments up to 1000 ppm (Fig. 6). Relative Sr variations in the Danian profiles are similar for both sections, except for ~100 ppm increases for samples at 0.350, 0.375, 0.400, and 0.700 m in MRL (Fig. 6). There is also a difference in the absolute concentrations between both sections, with values up to 100–200 ppm higher for the Gubbio sections. The MRL Mn concentration profile is similar, both in terms of absolute and relative variations, to the one at Gubbio (Figs. 5 and 6).

The smoothed (7 point moving average) elemental Ca, Fe, Sr, and Mn profiles for all the investigated Cretaceous-Paleogene sections (BOT, COH, MRL, FOE, FRO, and PTC) are shown in Figure 7. As an exception, the data set from FRO was not averaged because it contained just 14 measurements. All data are plotted in the distance domain, and because of varying sedimentation rates over the basin, certain features occurring before or after the Cretaceous-Paleogene boundary (which is the common 0 m reference stratigraphic level) are not positioned at the same stratigraphic levels. The Maastrichtian Ca (wt%) content varies for the different sections between 30 and 37 wt%. Right after the Cretaceous-Paleogene boundary clay layer, the Ca content peaks (i.e., ~40 cm of *Eugubina* limestone). This peak in Ca content is then followed by a minimum in all profiles around 1.00 m. The relative variations in the Ca content are mirrored by the Fe (wt%) profiles. The boundary clay measurement is clearly distinguishable in the FRO data as a peak in Fe and minimum in Ca content. The Maastrichtian BOT Fe profile shows more variation compared to the other Maastrichtian data (FOE, MRL, PTC), which is also the case for the BOT Sr curve. Moreover, the absolute Fe concentrations for BOT are more elevated compared to its parallel sections. Besides a common Fe peak around 1.00 m, only the PTC Fe profile shows a second pronounced peak before the 2.00 m level. The Sr (ppm) values of the Maastrichtian BOT section are 200–300 ppm higher than in FRO, FOE, MRL, and PTC sections, except for a sudden sharp increase in the PTC profile. All sections have an immediate strong decrease in Sr concentrations followed by a gradual increase upward. Anomalies on this predominantly monotonous increase in Sr concentrations include a small increase between levels 0.25 and 0.50 m (larger for MRL) and a sudden sharp increase for the PTC data at level 1.275 m to levels comparable to the Sr concentrations at level 3.50 m in COH. Levels of Mn (ppm) are comparable for all profiles for the Maastrichtian, with values between 300 and 400 ppm (Fig. 7). There is an increase in Mn concentrations in all profiles from ~350 to ~400 ppm from level –4.00 up to –2.00 m. Across the Cretaceous-Paleogene boundary, there is an ~200 ppm increase in Mn concentrations for all sections, but there is a larger variability in absolute concentrations for the Danian parts compared to the Maastrichtian parts. One Danian sample in the FRO profile (at 0.14 m) has values for Sr and Mn that are more similar to the Maastrichtian concentrations of Sr and Mn.

Stable Isotopes ($\delta^{13}C$ and $\delta^{18}O$)

Oxygen stable isotope ratio ($\delta^{18}O$) measurements on bulk pelagic limestone material from the Danian COH section (full

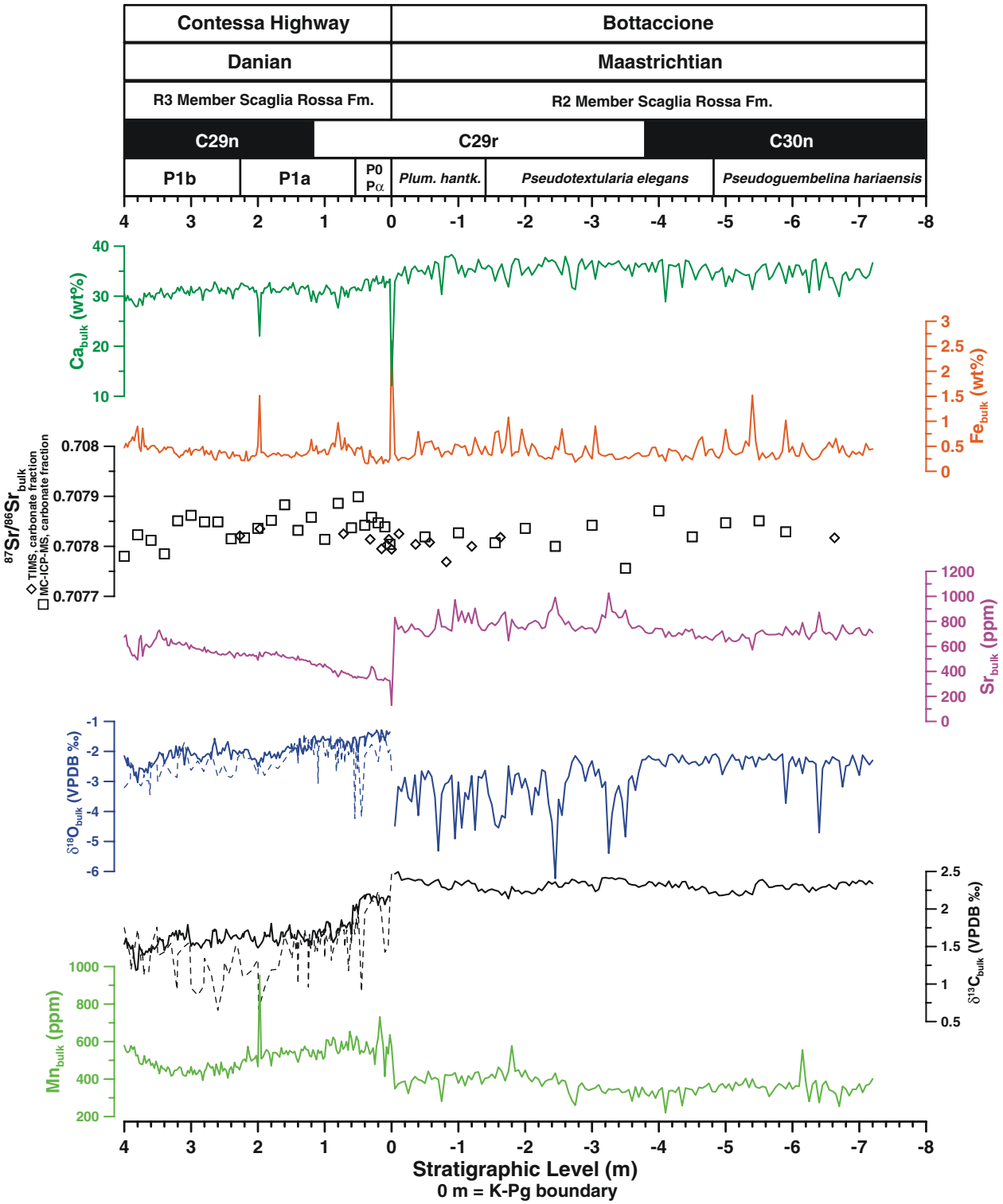

Figure 5. Stratigraphy and multiproxy records of the Gubbio sections (Maastrichtian Bottaccione [BOT] and Danian Contessa Highway [COH]). The magnetostratigraphy is according to Roggenthen and Napoleone (1977) for COH and to Lowrie et al. (1982) for BOT. The biostratigraphy for the COH section is from Coccioni et al. (2013), whereas that for the BOT section is from Coccioni and Premoli Silva (2015). Elemental concentration profiles of Ca, Fe, Sr, and Mn were measured with portable X-ray fluorescence (pXRF). Bulk stable isotopes ($\delta^{13}C$ and $\delta^{18}O$) from BOT are from Sinnesael et al. (2016a), whereas stable isotopes from COH were measured in this study (full lines) and Coccioni et al. (2012; dotted lines). All reported $^{87}Sr/^{86}Sr$ isotope results were measured during this study. *Plum. hantk.*—*Plummerita hantkeninoides*; K-Pg—Cretaceous-Paleogene; VPDB—Vienna Peedee belemnite; TIMS—thermal ionization mass spectrometry; MC-ICP-MS—multicollector–inductively coupled plasma–mass spectrometry.

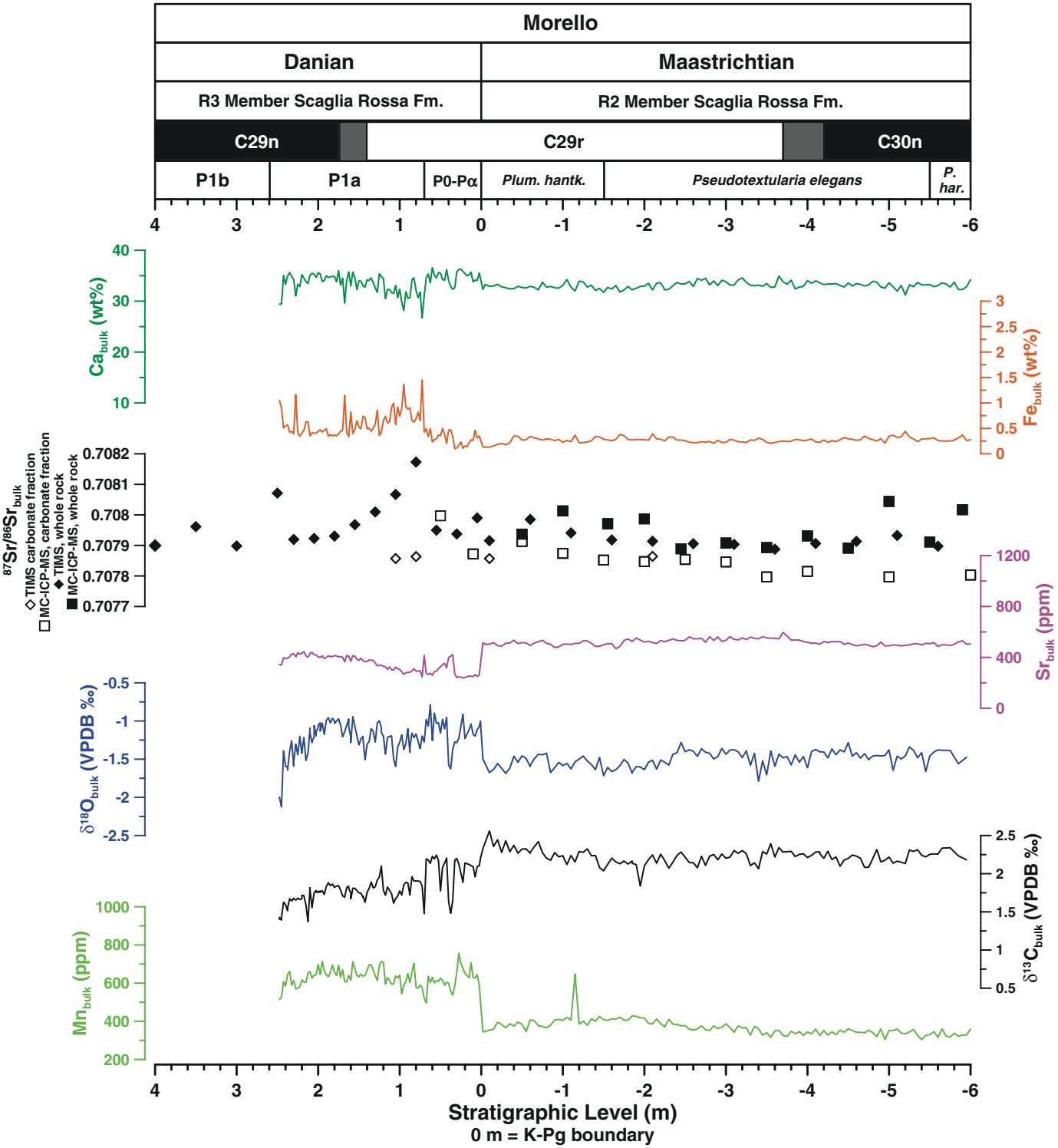

Figure 6. Stratigraphy and multiproxy records of the Morello section (all this study). *Plum. hantk.*—*Plummerita hantkeninoides*; *P. har.*—*Pseudoguembelina hariaensis*; K-Pg—Cretaceous-Paleogene; VPDB—Vienna Peedee belemnite; TIMS—thermal ionization mass spectrometry; MC-ICP-MS—multicollector–inductively coupled plasma–mass spectrometry.

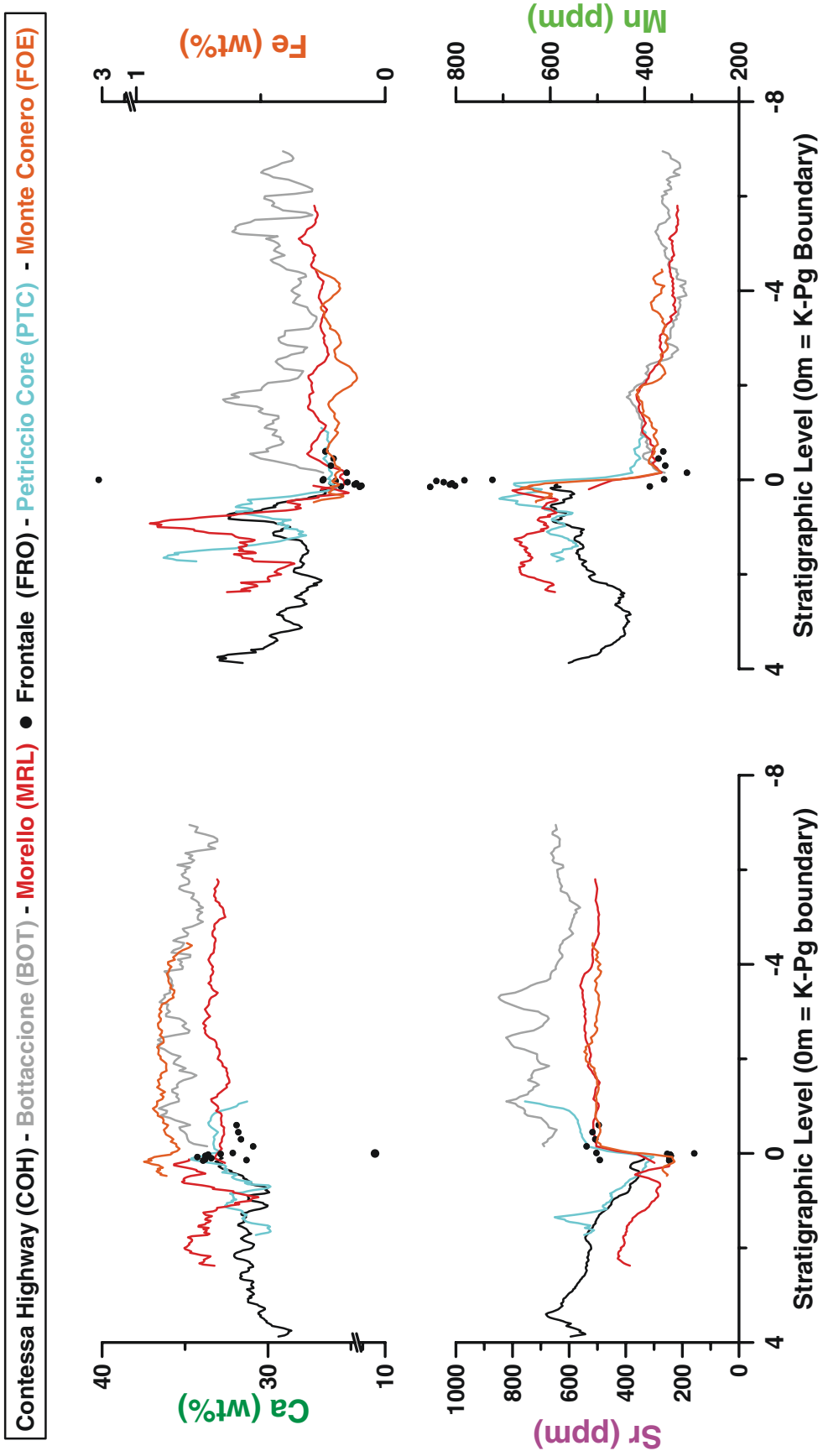

Figure 7. Smoothed (7 point moving average), except for the FRO data, elemental concentration profiles (Ca, Fe, Sr, and Mn) measured with a portable X-ray fluorescence (pXRF) spectrometer for six different Cretaceous-Paleogene sections in the Umbria-Marche basin. K-Pg—Cretaceous-Paleogene.

blue line on Fig. 5) have slightly less negative values compared to the results published in Coccioni et al. (2012; dotted blue line on Fig. 5). Particularly the pronounced negative peaks (>1‰) described by Coccioni et al. (2012) are not present. However, the main trend is still similar: a decrease over the Danian from ~–1.5‰ down to ~–2.5‰. Superimposed on this trend, the new record has local minima around levels 0.80, 2.00, and 3.80 m. The Maastrichtian MRL $\delta^{18}O$ values vary between −1.79‰ and −1.28‰, with an average of −1.50‰, with a small shift (0.2‰) in values around −1.4‰ to −1.6‰ at level −2.4 m (Fig. 6). These values are less negative compared to the BOT Maastrichtian data as published and discussed by Sinnesael et al. (2016a). Danian MRL $\delta^{18}O$ values start around −1.00‰, have a sharp decrease in values for the 0.35–0.40 m interval, have another local minimum around 1.00 m, and finally show a decreasing trend in the upper half meter. Compared to the BOT data, the MRL Maastrichtian data show much smaller amplitude variations and less negative values (Figs. 5, 6, and 8). Relative variations for both Danian $\delta^{18}O$ profiles are similar, but again the $\delta^{18}O$ values at MRL are less negative compared to Gubbio-COH (Figs. 5, 6, and 8).

The difference between the new (this study) and published (Coccioni et al., 2012) $\delta^{13}C$ data for the Danian COH are more pronounced compared to the $\delta^{18}O$ results (Fig. 5). There are no large (>1.00‰) negative excursions in $\delta^{13}C$ in the new data set. The profile of the new data set starts with lowermost Danian values of ~2.15‰ that remain stable until level 0.575 m. Then, a significant negative shift (~0.5‰) occurs, whereafter there is a slight decreasing trend from values of ~1.8‰ to ~1.4‰ to the top of the record. There is an ~0.3‰ negative excursion for samples 3.800, 3.825, and 3.850 m. Indeed, the Danian MRL $\delta^{13}C$ data start with stable values of ~2.10‰ followed by an ~0.5‰ shift at level 0.70 m and a slight decreasing trend (~1.9‰ to ~1.6‰) until the top of the measured section. In contrast with the $\delta^{18}O$ signals, the MRL and BOT Maastrichtian $\delta^{13}C$ data are much more alike in terms of relative variations and absolute values (Figs. 5, 6, and 8). Both profiles vary between 2.0‰ and 2.5‰ and have local minima roughly around levels −2.0 m and −5.0 m.

A cross-plot of the respective $\delta^{18}O$ and $\delta^{13}C$ ratios (Fig. 8) confirms some of these observations, but it additionally shows a bimodal distribution for the Danian samples. Most of the samples from both the COH and MRL profiles plot on a linear trend with $\delta^{13}C$ values between 1.5‰ and 2.0‰. However, some samples plot as a clearly distinguishable cluster with values between 2.0‰ and 2.5‰. For both data sets, these samples correspond to samples from the stratigraphic interval between the Cretaceous-Paleogene boundary and the ~0.5‰ drop in $\delta^{13}C$ values around 0.6 m (COH) and 0.7 m (MRL; Figs. 5 and 6). The linear trend of decreasing $\delta^{18}O$ values for decreasing $\delta^{13}C$ values is similar for both records. The three data points with the lowest values for both isotopic systems correspond with the 3.80–3.85 m COH Danian anomaly (Fig. 5). Furthermore, the anomalously (compared to MRL) negative $\delta^{18}O$ values for the Maastrichtian BOT are clearly distinguishable. Average Maastrichtian $\delta^{13}C$ values for MRL are also slightly lower (0.08‰) than for BOT.

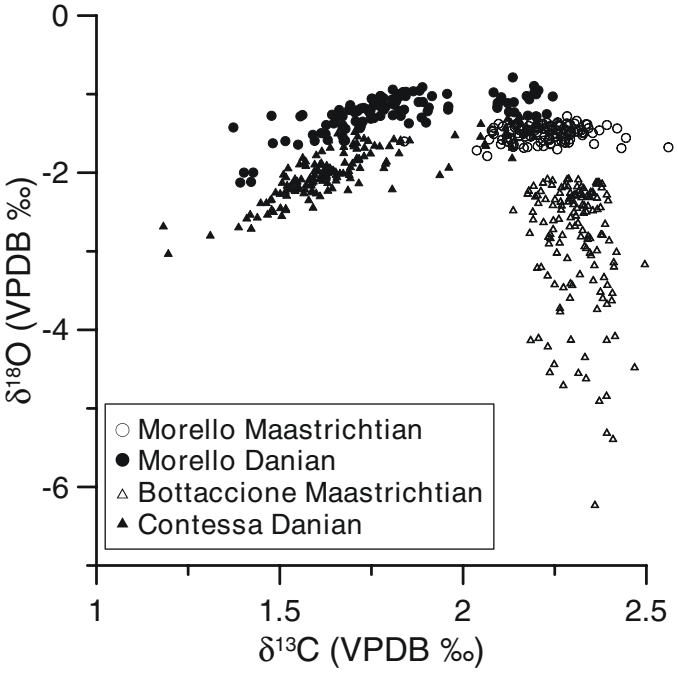

Figure 8. Cross-plot of bulk carbon and oxygen stable isotope ratios from the respective Maastrichtian and Danian sections of Morello and Gubbio (Bottaccione and Contessa Highway). VPDB—Vienna Peedee belemnite.

Hand-Sample μXRF and Stable Isotope ($\delta^{13}C$ and $\delta^{18}O$) Measurements

Four different subsamples (pure calcite vein, mixed calcite vein with matrix, mixed stylolite with matrix, and pure matrix) were taken from a hand sample containing clear calcite veins and stylolites (Fig. 9). The $\delta^{13}C$ ratios were statistically inseparable for all samples, while the samples containing calcite vein material showed lower $\delta^{18}O$ values. The pure calcite vein sample (−14.2‰) was ~12‰ more depleted than the surrounding pink matrix (−2.5‰). The mixed sample with some calcite vein material showed a value between these two end members, which suggests mixing, while the mixed sample containing stylolite material overlapped within the error with the pink matrix (Fig. 9). Micro-XRF mapping and line scanning across several stylolite sections showed clear enrichments in detrital elements like K, Fe, and Ti, and a reduction in Ca concentrations (Fig. 9). The exact opposite pattern was observed for the same measurements on the calcite vein. While the Sr concentrations were distinctly more elevated in the calcite veins, the Sr distribution for the stylolites was more complicated. In the calcite veins, the Sr enrichments coincided with decreases in K, Fe, and Ti. However, the μXRF mapping and line scanning showed an asymmetrical distribution of the Sr concentrations relative to the position of the detrital elements (Fig. 9).

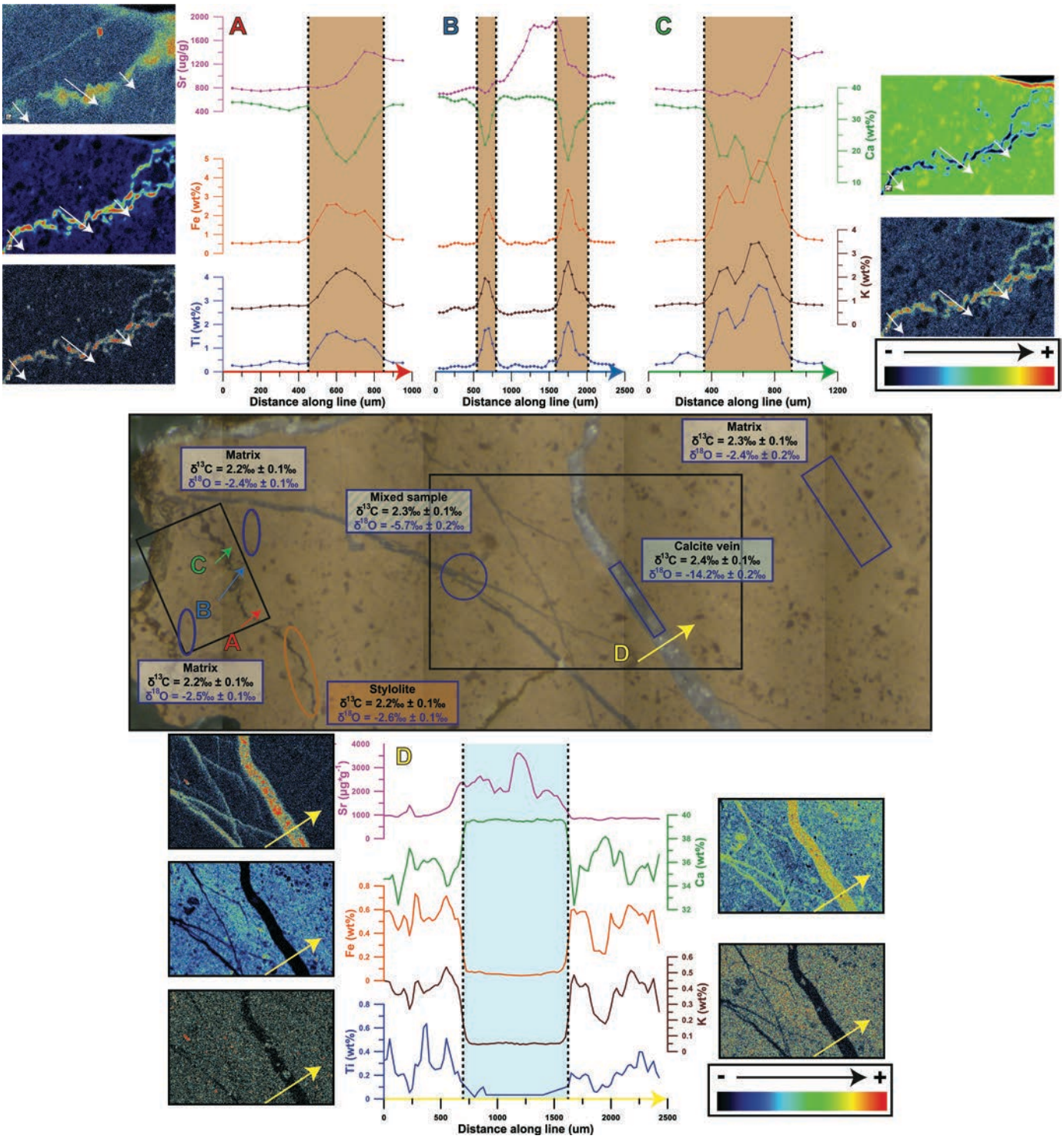

Figure 9. Micro–X-ray fluorescence mapping (semiquantitative maps), line scanning (quantified), and stable isotope ($\delta^{13}C$ and $\delta^{18}O$) analyses of a hand sample containing clear calcite veins and stylolites. This sample was taken around level −1.50 m from the Bottaccione section. In contrast to the pressure solution stylolites, the calcite veins are enriched in Ca and Sr and depleted in Fe, K, and Ti. The $\delta^{13}C$ signal overlaps within the error for all samples (pure calcite vein, mixed calcite vein with matrix, mixed stylolite with matrix, and pure matrix). The samples containing calcite vein material have lower $\delta^{18}O$ values.

Strontium Isotopes ($^{87}Sr/^{86}Sr$)

All strontium isotope ($^{87}Sr/^{86}Sr$) measurements for the Gubbio sections (BOT + COH) were done on the bulk carbonate fraction (Fig. 5). Both TIMS and MC-ICP-MS results overlapped, with larger variations for the latter ones (full range = 0.707899–0.707756). The average MC-ICP-MS $^{87}Sr/^{86}Sr$ value for this interval is 0.707834 and is in line with the geological time scale (GTS) 2012 compilation (McArthur et al., 2012). For this stratigraphic interval in Gubbio, there is no increasing or decreasing trend in the $^{87}Sr/^{86}Sr$ measured on the carbonate fraction (Fig. 5). The $^{87}Sr/^{86}Sr$ measurements on the MRL carbonate fraction overlap again between TIMS and MC-ICP-MS measurements and have an indistinguishable (within the MC-ICP-MS 2σ error of 0.000040) average value of 0.707834 compared to Gubbio (0.707857), but a larger range (0.707797–0.707997; Fig. 6). Whole-rock TIMS and MC-ICP-MS $^{87}Sr/^{86}Sr$ results for the Maastrichtian MRL section are in agreement with each other (except for two higher MC-ICP-MS values at levels −5.00 m and −6.00 m), and they are ~0.0001 higher than the measurements done on the carbonate fraction (Fig. 6). The Danian MRL whole-rock $^{87}Sr/^{86}Sr$ TIMS profile is characterized by a sharp increase at level 0.80 m, which is followed by a hyperbolic decrease to "pre-increase" whole-rock isotopic values at ~2.00 m (Fig. 6). The sample with a high $^{87}Sr/^{86}Sr$ value at MRL level 2.50 m was taken just above the ALE volcanic ash layer and might have been slightly contaminated with more radiogenic material. An $^{87}Sr/^{86}Sr$ isotope profile in the Umbria-Marche basin for the middle Campanian up to the early Ypresian, as measured in the Gubbio sections (Bottaccione and Contessa Highway) on the bulk carbonate fraction (TIMS), is shown in Figure 10. The fish teeth $^{87}Sr/^{86}Sr$ values generally fall within error of the associated bulk carbonate samples, which suggests that $^{87}Sr/^{86}Sr$ values of bulk carbonate samples are close to the original paleoceanographic value (Table DR3 [see footnote 1]). Values rise from the middle of the Campanian magnetochron C33n (0.707650 ± 0.000003) to a maximum in the Danian chron C29n (0.707831 ± 0.000008), and then decrease again to the youngest sample in the Ypresian chron C24r (0.707739 ± 0.000006). This profile is analogous to the GTS 2012 compilation by McArthur et al. (2012). The lower Danian maximum value is in accordance with the Gubbio MC-ICP-MS average value (0.70783) for the uppermost Maastrichtian–lower Danian interval. Measurements close to the Cretaceous-Paleogene boundary show more scatter compared to ones farther away from the boundary. Table DR3 contains other fragmentary $^{87}Sr/^{86}Sr$ data from other Cretaceous-Paleogene sections in the Umbria-Marche basin that are in close agreement with the profile shown in Figure 10.

$^{40}Ar/^{39}Ar$ Dating Contessa Highway ALE Volcanic Ash

The analyzed COH-ALE biotite grains were quite small, and the resulting data have multiple possible interpretations. However, given the paucity of available geochronology from this section, the data collected here do provide some constraint on the timing of sedimentation. After removing obvious xenocrysts, and grains that were substantially younger than the main population, the remaining population yielded an inverse variance weighted

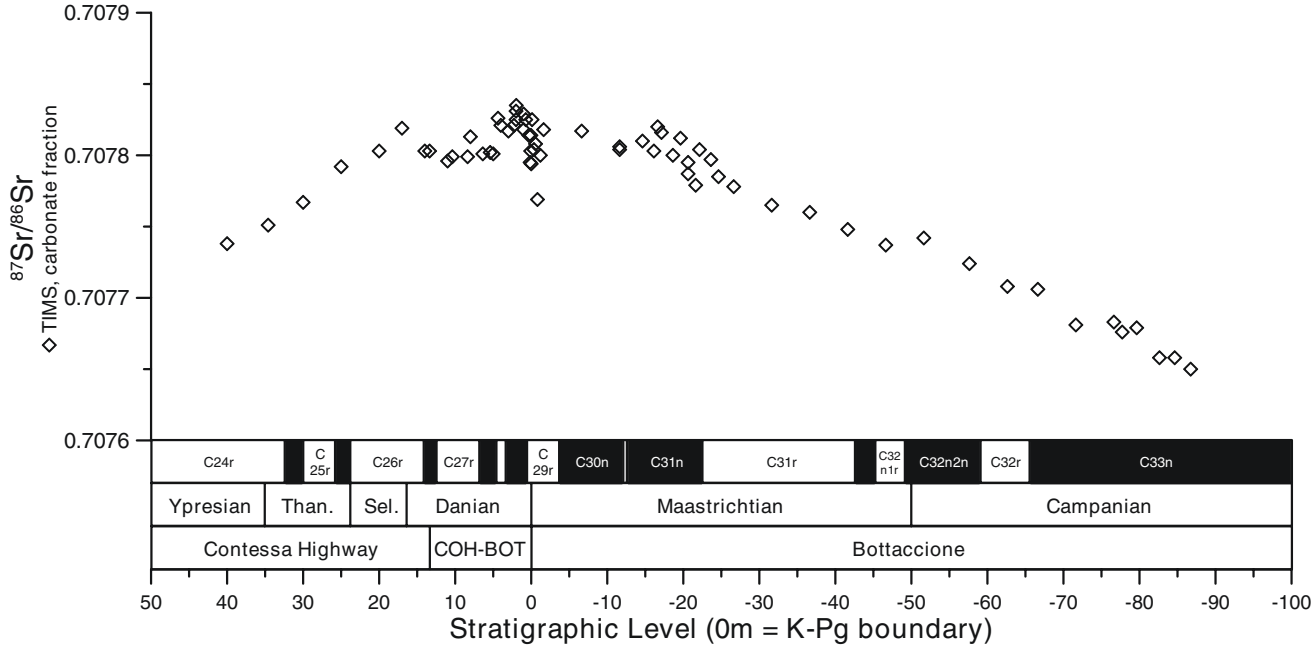

Figure 10. $^{87}Sr/^{86}Sr$ isotope profile in the Umbria-Marche basin for the middle Campanian up to the early Ypresian as measured in the Gubbio sections (Bottaccione and Contessa Highway) on the bulk carbonate fraction. TIMS—thermal ionization mass spectrometry; K-Pg—Cretaceous-Paleogene; Than.—Thanetian; Sel.—Selandian.

mean age of 64.8 ± 1.6 Ma (Fig. 11), which is younger than the age of the Cretaceous-Paleogene boundary (66.043 ± 0.043 Ma, according to Renne et al., 2013). This is consistent with the sampling location relative to the Cretaceous-Paleogene boundary at COH (+2.00 m). It should be noted that different recent calibrations of the $^{40}Ar/^{39}Ar$ system slightly affect the ages obtained; for reference, ages calculated using different parameters for each analyzed grain are provided in Table DR4 (see footnote 1). Given the small size of the biotite grains analyzed, it is possible that some of the anomalously young grains were affected by recoil (e.g., Paine et al., 2006), or possibly by outcrop contamination (Montanari, 1986).

DISCUSSION

Sedimentology and Geochemistry: Basinwide Robust Patterns

The sedimentological and geochemical analyses of several stratigraphically equivalent sections from the Umbria-Marche basin allow us to differentiate between basinwide and more local features. A pronounced difference in bedding style between the BOT (Figs. 2B and 2D) and MRL (Figs. 2A and 2C) sections is due to pseudobedding (sensu Alvarez et al., 1985). While the Maastrichtian average bedding thickness in MRL is ~30–40 cm, the apparent bedding in the BOT section (i.e., the pseudobedding) is much thinner than that (~5–10 cm) because of the presence of numerous bedding-parallel pressure solution planes, i.e., stylolites (e.g., as discussed in Sinnesael et al., 2016a). In comparison with all other investigated sections in this study, the BOT section shows more elevated concentrations of Sr and Fe (Fig. 7). These are most probably the effect of accidental sampling of calcite veins (enriched in Sr; Fig. 9) and stylolites (enriched in Fe; Fig. 9) in the BOT section while using a drill to collect sample powder (Fig. 2D; Sinnesael et al., 2018). The effect of sampling calcite veins is also reflected in the negative excursions in the bulk $\delta^{18}O$ signal from BOT (Figs. 4, 8, and 9). The base $\delta^{18}O$ values for both the Maastrichtian and Danian samples are less negative for MRL compared to the COH and BOT Gubbio sections (Fig. 8), independent of the negative bulk $\delta^{18}O$ excursions in BOT.

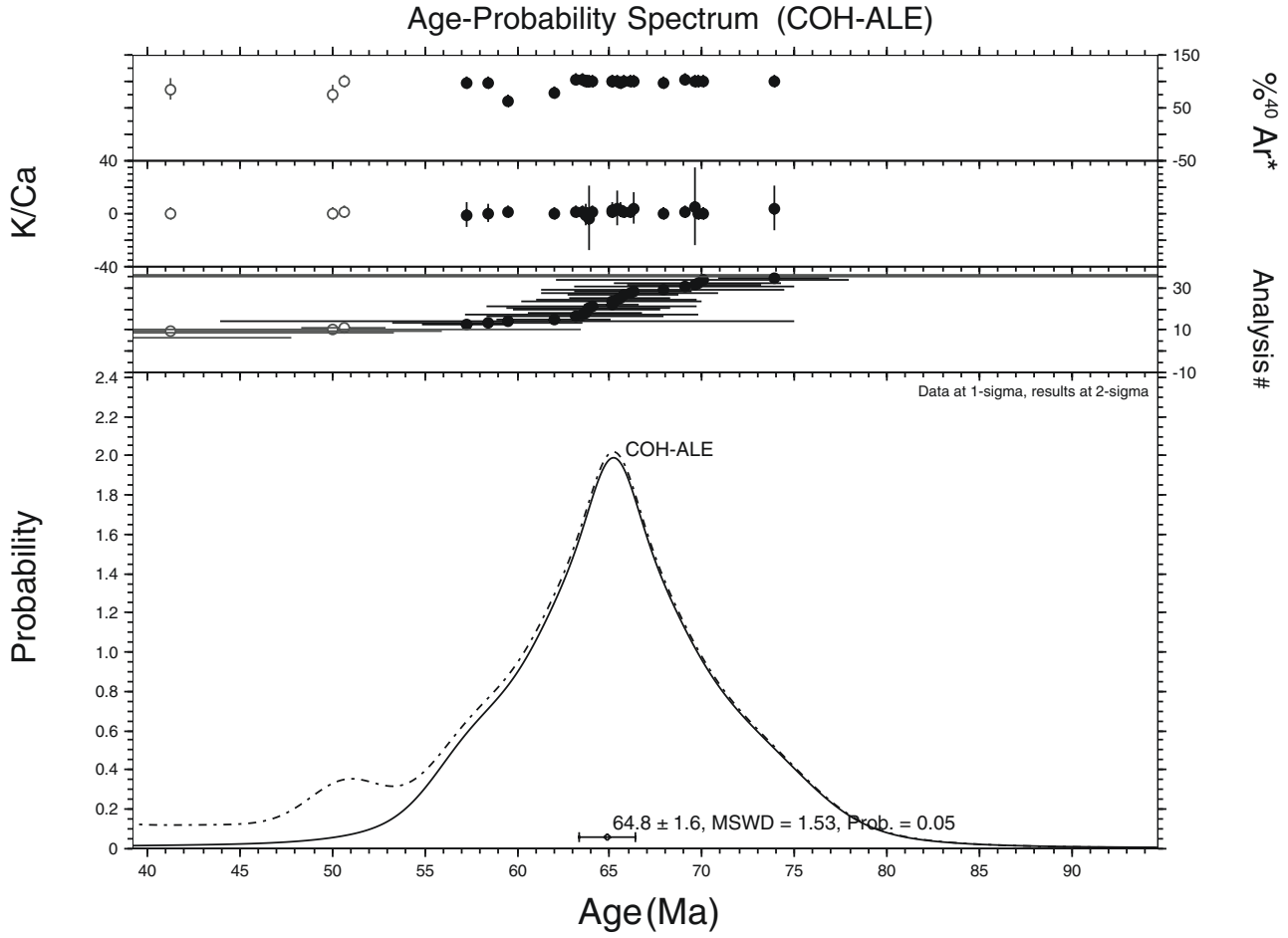

Figure 11. Results from $^{40}Ar/^{39}Ar$ dating of biotite grains from the "Livello Alessandro" (ALE) volcanic ash layer from the Contessa Highway (COH) section. MSWD—mean square of weighted deviates.

The combination of these geochemical observations, the fact that the MRL section is stratigraphically thicker than the Gubbio section (Table 1), the presence of the pressure solution features, and a less horizontal bedding angle in Gubbio suggest that the Gubbio sections were more affected by burial diagenesis that the MRL section. Robust features for the Maastrichtian records are the bulk carbonate $\delta^{13}C$ and Mn concentration profiles (Figs. 5–7). Most investigated Cretaceous-Paleogene boundary intervals are also characterized by the terminal Maastrichtian 20- to 30-cm-thick bleached white horizon, which contrasts with the typical pink color of the surrounding Maastrichtian and Danian pelagic limestones. The bleached horizon is not evident in the FOE section at Monte Conero (for location, see Fig. 1B), because this area of the paleobasin was located in the immediate proximity of a carbonate platform, a deep-marine environment that was characterized by relatively reducing conditions compared to the more oxidizing conditions in deeper and more distal areas of the paleobasin. Practically, the Maastrichtian and Danian Scaglia Rossa Formation limestones in the whole area of Monte Conero are not typically pink like in the rest of the paleobasin, but whitish or pale beige (Montanari et al., 1989; Montanari and Koeberl, 2000). The actual Cretaceous-Paleogene boundary clay is typically red in color with a thin reduced green sole (Montanari et al., 1983; Lowrie et al., 1990; Montanari, 1991), but it exhibits here a homogeneous ocher color and does not contain authigenic goethite like any other Cretaceous-Paleogene boundary clay in the rest of the basin (Montanari, 1991). This probably also explains why the Maastrichtian pelagic limestones in the FOE section have the lowest Fe and highest Ca concentrations compared to all other measured sections in the distal Scaglia Rossa basin (Fig. 7). The elevated Ca values for the BOT section might reflect a sampling bias caused by the sampling of calcite veins that are enriched in $CaCO_3$ (Figs. 7 and 9). Consistent geochemical features across the Cretaceous-Paleogene boundary for all records are the decrease in Sr and Ca concentrations, and the increase in Mn and Fe concentrations (Fig. 7). In the Danian profiles, the *Eugubina* limestone (~0.00–0.40 m) is typically characterized by a maximum in Ca concentration (Fig. 7). Also the marly interval (~0.60–1.10 m) corresponding with the Dan-C2 hyperthermal event is a reoccurring feature expressed as a local minimum in Ca and maximum in Fe (Fig. 7; Coccioni et al., 2010).

Besides these large-scale overall observations, other interesting small-scale features appear from this high-resolution geochemical study. One of the pXRF measurements of the FRO section was taken from a large bioturbation burrow filled with Maastrichtian pelagic sediment, within the *Eugubina* limestone, ~10 cm above the Cretaceous-Paleogene boundary (see fig. 5.7.6.10b at p. 235 *in* Montanari and Koeberl, 2000). In this case, the Sr and Mn contents correspond exactly with the Maastrichtian bulk values—which are substantially different before and below the Cretaceous-Paleogene boundary—and so this demonstrates that bioturbation crossed the Cretaceous-Paleogene boundary, causing some degree of vertical mixing (Fig. 7). Another anomalous feature, compared to the other parallel sections, is the sharp and sudden increase in Sr concentrations at level 1.275 m for the PTC core (Fig. 7). The absolute values of this Sr anomaly correspond to the peak concentrations around level 3.50 m in COH. Putting all elemental pXRF analyses together, it seems that there is a Danian hiatus of ~2 m in the PTC core, which was not recognized earlier. Samples 0.350, 0.375, 0.400, and 0.700 m in MRL are characterized by clear geochemical anomalies: lower $\delta^{13}C$ and $\delta^{18}O$ values and higher Sr concentrations (Fig. 6). Interestingly, these anomalies do not show up significantly in the Mn data, hinting toward the potential diagenetic signature of the Mn signal. Field inspections of these levels with a hand lens have already suggested a potential turbiditic origin for these intervals (e.g., Bice et al., 2007). Small turbidites at similar levels are also visible in the FOE section, but they were not analyzed in this study with the pXRF exactly because they were clearly turbiditic. The geochemical anomalies for the MRL samples now confirm their turbiditic origin. These results illustrate how the relative fast and cheap chemostratigraphic application of pXRF measurements can be of added value. In summary, the most robust observations for this stratigraphic interval in the Umbria-Marche basin are: (1) the changes across the Cretaceous-Paleogene boundary, (2) the occurrence of the Cretaceous-Paleogene boundary clay layer, *Eugubina* limestone, and Dan-C2 marly interval, and (3) the different diagenetic history between the Morello and Gubbio sections.

Event Stratigraphy

Deccan Volcanism

Establishment of robust basinwide sedimentological and geochemical correlations allows for in-depth evaluation of the global events in this stratigraphic interval, including Deccan volcanism, the Cretaceous-Paleogene boundary and recovery, and the Dan-C2 hyperthermal event. One of the most compelling geochemical tracers of Deccan volcanism in the sedimentary archive is a drop in the $^{187}Os/^{188}Os$ isotopic ratio a few hundred thousand years prior to the Cretaceous-Paleogene event (Ravizza and Peucker-Ehrenbrink, 2003; Ravizza and VonderHaar, 2012). This drop has also been identified 5–6 m below (~300–400 k.y. before) the Cretaceous-Paleogene boundary in the BOT section (Robinson et al., 2009). Benthic foraminiferal $\delta^{18}O$ values (Li and Keller, 1998; Barnet et al., 2017), and to some extent bulk carbonate $\delta^{18}O$ records (Thibault et al., 2016a) and other temperature proxies (Woelders et al., 2018), also show a clear warming a few hundred thousand years before the Cretaceous-Paleogene boundary. The bulk carbonate $\delta^{18}O$ record from BOT (Fig. 5), which was hypothesized by Sinnesael et al. (2016a) to potentially reflect Deccan global warming, is shown to be heavily affected by the sampling of diagenetic calcite veins and therefore does not support such interpretation (Fig. 9). Bulk carbonate $\delta^{18}O$ values for MRL shift to slightly lower values (0.20‰; Fig. 6) around −2.5 m, but this shift is small compared to the measurement error ($1\sigma = 0.10‰$) and the $\delta^{18}O$ shift in other bulk records (e.g., ~0.5‰; Thibault et al., 2016a). A basinwide increase in bulk

Mn concentrations ~300 k.y. prior to the Cretaceous-Paleogene boundary (Figs. 5, 6, and 7) might indicate a global increase in hydrothermal activity (e.g., Le Callonec et al., 2014). Elevated Hg/total organic carbon (TOC) ratios at certain stratigraphic levels in BOT have also been suggested to be useful identifiers of the different pulses of Deccan volcanism (Sial et al., 2016). However, the suggested stratigraphic correlations of these Hg/TOC peaks are debated (e.g., Smit et al., 2016; Mukhopadhyay et al., 2017). All things considered, the $^{187}Os/^{188}Os$ record at BOT is still the only convincing geochemical record of Deccan volcanism in the Umbria-Marche basin sedimentary succession.

Extinction and Recovery

The drop and following increase in bulk Sr concentrations across the Cretaceous-Paleogene boundary represent a robust pattern in all investigated sections in the Umbria-Marche basin (Figs. 5–7). The fact that the Sr profile does not correlate with the terrigenous components (e.g., Fe concentrations) suggests that the bulk Sr concentrations mainly reflect the Sr content of the $CaCO_3$ (calcite) components of the bulk sediments (Figs. 5–7). This is also indicated by the similarity of records between Sr concentrations and Sr/Ca ratios (see Table DR1 [footnote 1]; Sinnesael et al., 2018). The sudden decrease in Sr concentrations across the Cretaceous-Paleogene boundary was observed earlier in the BOT section by Alzeni et al. (1981) and Renard et al. (1982) and in the Spanish Caravaca section by Smit and ten Kate (1982). Several mechanisms were proposed to potentially explain this shift: changes in relative local sea level, a change in the source area of clastic supply, different diagenetic alteration of clay minerals due to different sedimentation rates, variations in the Sr/Ca ratio of seawater, variations in seawater salinity and/or temperature, and metabolic effects on biochemical fractionation of strontium by calcifying microorganisms (foraminifera and nannoplankton; Alzeni et al., 1981; Renard et al., 1982). However, none of these hypotheses was supported by conclusive evidence. Interestingly, a similar Sr/Ca profile has been measured in the same stratigraphic interval in the Scaglia Rossa Formation of the Forada section in the southern Alps of northern Italy (Fornaciari et al., 2007). Fornaciari et al. (2007) demonstrated that the Sr/Ca ratio decrease coincides with a drastic decrease in coccolithophorid production after the Cretaceous-Paleogene mass extinction and that the increase in Sr/Ca goes hand in hand with the recovery of these biogenic carbonate producers (as measured in total abundance as well as taxonomic diversity). This observation is in line with the hypothesis that the coccolith Sr/Ca ratio may be a proxy for coccolithophorid productivity (Stoll and Schrag, 2000). Other factors could also have an influence on coccolithophorid Sr/Ca ratios, such as temperature, dissolution, and growth rate (Stoll and Schrag, 2000; Rickaby et al., 2002; DePaolo, 2011). The studied Dan-C2 hyperthermal (potential warming and carbonate dissolution) marly intervals in the Umbria-Marche basin show a small decrease in total Sr concentrations, but not in the Sr/Ca ratios, suggesting that temperature and dissolution indeed had a minor influence on the Sr/Ca ratio, as stated by Stoll and Schrag (2000) (Figs. 5–7; Table DR1 [see footnote 1]). Assessing the actual growth rate of these organisms across the Cretaceous-Paleogene boundary is difficult because of large variations in taxonomy, ecology, etc. Nevertheless, the fact that lower Danian foraminifera and coccolithophores are much smaller than Maastrichtian ones might suggest a decrease in growth rate, though small test sizes do not necessarily imply slow growth rates (e.g., Gardin and Monechi, 1998; Bernaola and Monechi, 2007; Fornaciari et al., 2007).

This major drop in biogenic carbonate productivity can also explain the slower accumulation rates for the Danian compared to the Maastrichtian (e.g., Arthur and Fischer, 1977; Smit, 1982; Mukhopadhyay et al., 2001; Fornaciari et al., 2007; Gardin et al., 2012; Coccioni et al., 2013; Sinnesael et al., 2016a). Assuming this mechanism is correct, one might expect to see a comparable Sr/Ca signal in sedimentary and stratigraphically equivalent sections (in which the carbonate fraction is dominated by the nannofossil component). However, many other Cretaceous-Paleogene boundary sections consist of different types of sediments and commonly have pronounced lithological differences before and after the Cretaceous-Paleogene boundary, complicating the comparison of bulk measurements. The Spanish Zumaia section, for instance, has a documented Sr/Ca drop across the Cretaceous-Paleogene boundary (Margolis et al., 1987), but in contrast with the Umbria-Marche sections, the basal Danian P0-Pa zone in this section is marly, whereas in the Umbria-Marche basin, this stratigraphic interval is represented by the hard, 96–97 wt% $CaCO_3$ *Eugubina* limestone (e.g., Sinnesael et al., 2016a). A sudden drop in bulk Sr/Ca and a rise over the lower Danian part of the section are also found for the Spanish Caravaca Cretaceous-Paleogene boundary section (Kaiho et al., 1999; Smit and ten Kate, 1982). Although the stratigraphic resolution does not allow evaluation of the presence of a smooth increase in Sr values, the bulk measurements of Upper Maastrichtian and Lower Paleocene samples from the European Biarritz, Caravaca, Gubbio, and Zumaia sections (Smit and ten Kate, 1982), and the Sr concentrations of several, mainly North Atlantic, Deep Sea Drilling Project (DSDP) sites (Renard, 1986) show lower Sr values above the Cretaceous-Paleogene boundary compared to Upper Maastrichtian concentrations. All these studies reporting a large change in Sr/Ca over the Cretaceous-Paleogene boundary were located in the paleo-Tethys and North Atlantic Ocean. To our knowledge, no similar Sr profiles have been documented outside the Tethys and North Atlantic Ocean to date (e.g., Zachos and Arthur, 1986; Schulte et al., 2006). This might be explained by the nonhomogeneous distribution in time and space of the Cretaceous-Paleogene nannoplankton extinction patterns and recovery rates (e.g., Jiang et al., 2010; Hull et al., 2011). Jiang et al. (2010), for example, stated that extinction rates in the Northern Hemisphere were higher compared to the Southern Hemisphere, and population recoveries were much faster for the latter hemisphere. In this scenario, it is not necessarily the case that all worldwide Cretaceous-Paleogene boundary sections with similar pelagic carbonate sedimentology as in the Umbria-Marche basin have a comparable change in

Sr/Ca over the Cretaceous-Paleogene boundary and during the earliest Paleocene.

Dan-C2 Hyperthermal Event

Quillévéré et al. (2008) were the first to suggest the existence of the first Paleogene hyperthermal event, the Dan-C2 (top of magnetochron C29r in Ocean Drilling Program [ODP] Site 1049). Soon after, Coccioni et al. (2010) identified the Dan-C2 in the COH section. The Dan-C2 event in COH is lithologically represented by an ~30-cm-thick (0.6–0.9 m levels) marly interval marked by bulk $\delta^{13}C$ and $\delta^{18}O$ negative shifts accompanied with changes in calcareous nannofossils and foraminiferal fauna (Coccioni et al., 2010). The elevated ^{3}He concentrations for this same interval suggest condensation, for example, by carbonate dissolution, as is common for hyperthermal events (Fig. 12; Mukhopadhyay et al., 2001). In addition, the $^{87}Sr/^{86}Sr$ signature of the whole-rock MRL measurements is more radiogenic (Fig. 6). In contrast with the previous bulk $\delta^{13}C$ record for COH (Coccioni et al., 2012), the new COH record shows a clear drop in $\delta^{13}C$ values at the start of this marly interval (Fig. 5). The same

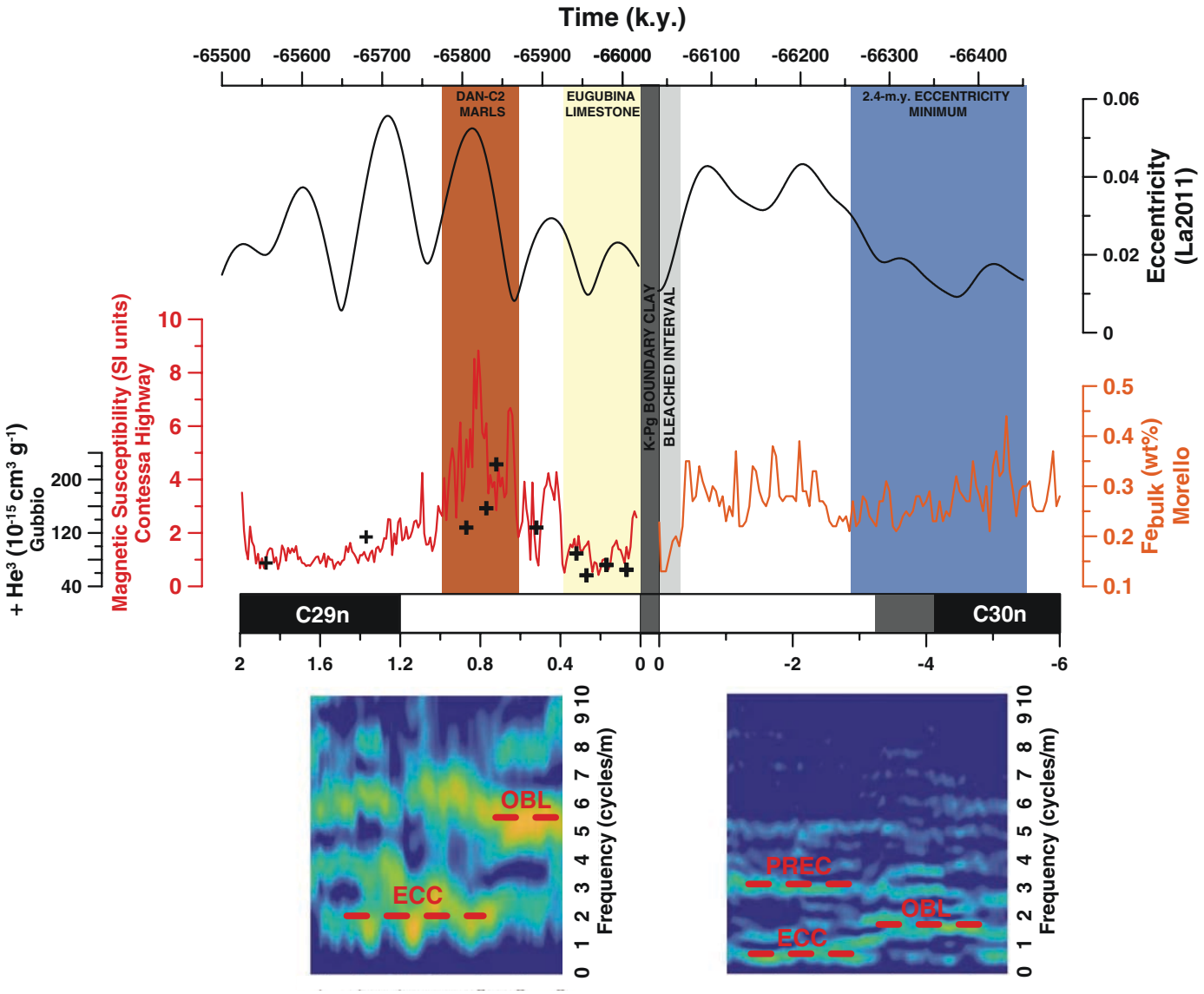

Figure 12. Cyclostratigraphic interpretation of the Cretaceous-Paleogene (K-Pg) boundary event stratigraphic interval. The La2011 eccentricity solution is shown in the time domain with 20 k.y. missing at the Cretaceous-Paleogene clay layer (Mukhopadhyay et al., 2001; Laskar et al., 2011a, 2011b; Renne et al., 2013; Dinarès-Turell et al., 2014). Proxies for detrital input with the highest available spatial resolution (every 5 cm Fe portable X-ray fluorescence data from the Morello Maastrichtian [this study] and every 1 cm magnetic susceptibility data from COH [Sinnesael et al., 2016a]) were selected for evolutionary fast Fourier transformation analysis. Plotted ^{3}He data are from Mukhopadhyay et al. (2001). OBL—obliquity; ECC—eccentricity; PREC—precession.

pattern is also observed in the MRL section (Fig. 6). The bulk stable carbon and oxygen cross-plot from the Danian MRL and COH data also illustrates that this transition toward the Dan-C2 marls is the division between two clusters (for both sections) in the data (Fig. 8). The first cluster has $\delta^{13}C$ values higher than 2.00‰ and does not show any trend in the $\delta^{18}O$-$\delta^{13}C$ space. The second cluster has $\delta^{13}C$ values lower than 2.00‰ with a linear trend of decreasing $\delta^{13}C$ values with decreasing $\delta^{18}O$. A first explanation could be differential diagenesis between both intervals, as isotopic measurements were performed on bulk material. An alternative clarification could be that the covariation between $\delta^{13}C$ and $\delta^{18}O$ represents a true climatic signal. Stable isotope analyses ($\delta^{13}C$ and $\delta^{18}O$) on benthic foraminifera for Eocene hyperthermals have shown these linear trends between $\delta^{13}C$ and $\delta^{18}O$ as well (Stap et al., 2010; Lauretano et al., 2015). These studies suggest that warming (hyperthermals, reflected in $\delta^{18}O$ signal) might go hand in hand with perturbations of the carbon cycles, such as, for example, negative $\delta^{13}C$ peaks, because of the release of isotopically light carbon, events that might be associated with carbonate dissolution (e.g., Zachos et al., 2010; Littler et al., 2014). Stable isotope measurements in this study were, however, done on bulk material with likely a diagenetic imprint, which prevents direct comparison with the previous studies on foraminifera. Nevertheless, this multiproxy study does support the hypothesis that this marly interval (~0.60–1.00 m) represents the Dan-C2 hyperthermal event in this basin. The exact (global?) nature, severity, and extent of this event can only be evaluated by further studies (e.g., Westerhold et al., 2011; Gilmour et al., 2013, 2014; Jolley et al., 2017).

Temporal Framework and Astronomical Climate Forcing

The sedimentology of the lowermost Danian strata in the Umbria-Marche basin is highly variable in facies over a short stratigraphic interval, making the precise and accurate construction of its temporal framework challenging (e.g., as discussed in Sinnesael et al., 2016a). The strata before the Cretaceous-Paleogene boundary clay layer are bleached and geochemically altered but do not show different (rates of) sedimentation compared to the underlying typically pink Maastrichtian limestones of the R2 member of the Scaglia Rossa Formation (Montanari et al., 1989; Lowrie et al., 1990; Sinnesael et al., 2016a). With the impact at the Cretaceous-Paleogene boundary, this pelagic carbonate sedimentation was abruptly interrupted, and the Cretaceous-Paleogene boundary clay was deposited (Alvarez et al., 1980). The amount of time represented within the Cretaceous-Paleogene boundary clay is estimated to be in the order of 10 k.y. (e.g., Mukhopadhyay et al., 2001). On top of the boundary clay, there is the ~45-cm-thick, hard and fine-grained *Eugubina* limestone. This limestone interval is followed by a marly interval some ~50–60 cm thick, which then again is followed by a pink limestone interval that becomes more marly again toward the 3–4 m interval. In the middle of this complex interval, there is the ALE volcanic ash layer (2.00 m above the Cretaceous-Paleogene boundary in the COH section and 2.45 m in the MRL section). Earlier fission-track analysis on 18 selected apatite crystals gave a rough and unrealistic age for the ALE of ca. 90 Ma (Odin et al., 1992). The same study reported the extraction of small zircons, which were deemed unsuitable for dating, and recovered biotite flakes, which, although euhedral, in some cases in booklets, seemingly fresh and with no signs of alteration, were regarded to be too small for further separation and utilization for radioisotopic dating. In this study, the new $^{40}Ar/^{39}Ar$ age of the small biotite flakes of 64.8 ± 1.6 Ma appears to be more accurate, considering its position relative of the Cretaceous-Paleogene boundary ($^{40}Ar/^{39}Ar$ dated at 66.043 ± 0.043 Ma by Renne et al., 2013), but it is unfortunately not precise enough to be useful to untangle the precise time line (~10^4 k.y. on orbital time scales) of the complex post–Cretaceous-Paleogene sedimentary successions.

Classical magnetostratigraphy and biostratigraphy are the backbone of the temporal calibration of this stratigraphic interval (Roggenthen and Napoleone, 1977; Lowrie et al., 1982; Gardin et al., 2012; Coccioni et al., 2013; Coccioni and Premoli Silva, 2015), but cyclostratigraphic analyses have the additional advantage of providing time information between discrete (boundary) events (Husson et al., 2014; Galeotti et al., 2015; Sinnesael et al., 2016a, 2016b). Assuming no major sudden changes in the sedimentation rate, for which there are no sedimentological indications, Sinnesael et al. (2016a) documented in the Maastrichtian BOT section a shift from a strong obliquity signal for the ~–7.2 to –4.0 m interval toward a predominant precession and eccentricity imprint for the uppermost Maastrichtian interval (–4.0 to 0 m). Interestingly, Thibault et al. (2016b) suggested changes in sedimentation rate related to the Deccan event in a similar stratigraphic interval for the Tunisian Elles section. However, in the Umbria-Marche basin sections, there are no indications for substantial changes in sedimentation rate in this interval. The sliding FFT of the Maastrichtian pXRF MRL Fe data shows the same pattern (Fig. 12): an obliquity component (~0.6 m period, 1.7 m^{-1} frequency) for the –6.00 to 3.00 m interval, which transitions toward a coupled precession (~0.3 m period, 3.0 m^{-1} frequency) and eccentricity (~1.6 m period, 0.7 m^{-1} frequency) imprint for the upper half of the Maastrichtian interval. The ratios between these periodicities match well with the ratios of the estimated durations of precession and obliquity for 66.0 Ma (18.7 k.y., 22.5 k.y., and 39.5 k.y., respectively; Berger et al., 1992). This interpretation implies an average upper Maastrichtian sedimentation rate for the MRL section of ~15 m $m.y.^{-1}$, which is considerably higher than the one used for the parallel interval in BOT by Sinnesael et al. (2016a), i.e., 10.7 m $m.y.^{-1}$. One explanation is that the Gubbio sections are generally more condensed than the MRL section (Table 1), but this ~1.15 factor difference does not explain the full discrepancy. An additional explanation is the accidental sampling of stylolite material in the BOT series, which could have caused some deviations in the analyzed signal of the detrital proxies like Fe and magnetic susceptibility (see earlier discussion). However, the general pattern of the shift from an obliquity-dominated pattern toward precession-eccentricity is robust.

Cyclostratigraphic work on several sections worldwide (Zumaia, Sopelana, Shatsky Rise, and Walvis Ridge) suggests that the La2011 eccentricity solution as calculated by Laskar et al. (2011, La2011) is the one that best matches the data for the Danian (Dinarès-Turell et al., 2014). This solution has a 405 k.y. eccentricity minimum coinciding with a 2.4 m.y. eccentricity minimum between 66.45 and 66.25 Ma. Using the 66.043 Ma $^{40}Ar/^{39}Ar$ age from Renne et al. (2013) and taking the 3 m interval with a sedimentation rate of 15 m m.y.$^{-1}$ (3 m divided by 15 m m.y.$^{-1}$ = 0.2 m.y. duration) gives an age for the obliquity-precession transition of 66.243 Ma—therefore coinciding with the 2.4 m.y. eccentricity interval of the La2011 eccentricity solution within a few thousand years. This interpretation supports the Dinarès-Turell et al. (2014) interpretation concerning the locations of 2.4 m.y. eccentricity minima for this stratigraphic interval. Such minimal eccentricity configuration can be a good explanation for the dominant obliquity cycle for this interval. This understanding complements the initial hypothesis by Sinnesael et al. (2016a) that this transition would have been caused by changing climate sensitivity resulting from coincident global warming caused by Deccan volcanism. Amplified carbon cycle sensitivity to orbital precession during the Deccan greenhouse warming was also suggested by Barnet et al. (2017). One proxy to establish this amplified sensitivity in this study is the Fe intensity data from ODP Site 1262 (Walvis Ridge, South Atlantic), which was originally published in Westerhold et al. (2008). In contrast with the available data from the Umbria-Marche basin, this data set spans a longer stratigraphic interval, which allows us to test if this obliquity-precession transition also occurred for this section and additionally test the extent of the obliquity-dominated interval (assuming precession is dominant once not in the 2.4 m.y. eccentricity minimum). The sliding FFT of these Fe intensity data for the uppermost Maastrichtian (not shown in this paper) indeed shows a transitional increase in obliquity power—assuming no significant changes in sedimentation rate (e.g., Thibault et al., 2016b)—for this interval (223–225 m meter composite depth [mcd] interval using a window size of 4 m). Time-series analysis of the same data according to the age model of Barnet et al. (2017) shows no power in the eccentricity frequency range for its 66.2–66.4 Ma interval, which fits with the hypothesis of a 2.4 m.y. eccentricity minimum location. However, no clear obliquity is visible in this interval according to this age model, and there is a shift to higher frequencies in the precession band, which suggests potential tuning of actual obliquity cycles as precession cycles. The same approach was applied to the magnetic susceptibility data from the upper Maastrichtian in Zumaia (data from Batenburg et al., 2012, 2014), and a similar pattern was visible in that case (interpreted obliquity component imprint in the 5–10 m interval below the Cretaceous-Paleogene boundary interval). When analyzing large stretches of time (e.g., almost the entire Maastrichtian in Batenburg et al., 2012, 2014), such small-scale difference are more difficult to detect by spectral analysis for several reasons (e.g., the focus is on the integrated spectrum of the whole signal, and relative larger window sizes in the moving window approach will smooth out small-scale variations). In conclusion, the integration of these data and interpretation from different sections suggest that there is a 2.4 m.y. eccentricity minimum interval, which has a dominant expression in obliquity signals (except in the unlikely case that there are coinciding changes in sedimentation rate in all different sites) that last for about ~200 k.y. (ages ca. 66.25–66.45, assuming a Cretaceous-Paleogene boundary age of 66.043 Ma). With the same assumptions, this interval includes the C30n/C29r magnetostratigraphic boundary in all sections, which is cyclostratigraphically dated in the MRL section at an age of 66.32 Ma. The results from our cyclostratigraphic interpretations for C29r (Fig. 12) are in agreement with the most recent $^{40}Ar/^{39}Ar$ geochronologic constraints by Sprain et al. (2018).

Current cyclostratigraphic interpretations for the lowermost Danian are debated in the Gubbio sections (Husson et al., 2014; Galeotti et al., 2015; Sinnesael at al., 2016a, 2016b) and elsewhere (e.g., the post–Cretaceous-Paleogene boundary "Strange Interval" in Westerhold et al., 2008; Hilgen et al., 2015). Can the complex lowermost Danian chronology be resolved by combining a cyclostratigraphic interpretation for the Maastrichtian and location of the Cretaceous-Paleogene boundary with an eccentricity solution (i.e., La2011)? To address this, the 1-cm-resolution magnetic susceptibility record from COH (published in Sinnesael et al., 2016a) was reinvestigated in detail using the sliding FFT technique (Fig. 12). The lower part of the stratigraphic interval (0.0–0.8 m) shows a stronger imprint of an ~0.18-m-thick periodicity (5.5 m^{-1}), and the upper part (0.8–2.0 m) shows a stronger imprint of an ~0.44-m-thick periodicity (2.3 m^{-1}). Admittedly, the changing sedimentology makes robust interpretations difficult, but the current best interpretation (respecting the detailed biostratigraphy and magnetostratigraphy) is the association of the ~0.18 m periodicity with obliquity and the ~0.44 m period with short (100 k.y.) eccentricity (Fig. 12). Husson et al. (2014) similarly identified a 0.17 m obliquity component and 1.75-m-thick 405 k.y. eccentricity component for the lowermost Danian in COH for the whole interval, but they did not specify the spatial distribution of the relative occurrences of these components. Again, could a potential obliquity imprint be explained by the relative position of being in a 405 k.y. eccentricity minimum close to a 2.4 m.y. eccentricity minimum? This interpretation results in an average sedimentation rate of ~4.5 m m.y.$^{-1}$, which is in agreement with previous studies (e.g., Sinnesael et al., 2016a, 2016b). In contrast to the Maastrichtian part of the section, the sedimentology is variable in the lowermost Danian, and relatively high changes in sedimentation rate over the stratigraphic interval cannot be totally excluded. The large change in sedimentation rate across the Cretaceous-Paleogene boundary is well documented (e.g., see above; Arthur and Fischer, 1977; Smit, 1982; Mukhopadhyay et al., 2001; Gardin et al., 2012; Coccioni et al., 2013; Sinnesael et al., 2016a).

Following the cyclostratigraphic interpretations presented in this study for both the Maastrichtian and Danian in the

Umbria-Marche basin, the stratigraphic location of the Dan-C2 hyperthermal event coincides with the first pronounced short eccentricity maximum in a 405 k.y. maximum after a 2.4 m.y. eccentricity minimum (Fig. 12). This is the same orbital setting as for the occurrence of the Paleocene-Eocene thermal maximum and Elmo hyperthermal events (Lourens et al., 2005). Identical events and corresponding astronomical imprints were identified in the Contessa Road section of the Umbria-Marche basin (Galeotti et al., 2010; Laurin et al., 2016). Although the Dan-C2 event is less large in terms of global climatic perturbation compared to the Elmo and Paleocene-Eocene thermal maximum, the astronomical imprint could be a hint that it is an actual hyperthermal event, and that eventually the occurrence of other intervals characterized by marly intervals and negative $\delta^{13}C$ excursions was astronomically paced. Examples could be the top- C27n event or latest Danian event (LDE) and the low-C27r, which are recognized as well as in the Umbria-Marche basin (e.g., Coccioni et al., 2012; Galeotti et al., 2015) as elsewhere (e.g., Dinarès-Turell et al., 2014; Hilgen et al., 2015).

CONCLUSIONS

This basinwide multiproxy study of the Cretaceous-Paleogene boundary event stratigraphy in the Umbria-March basin demonstrates the successful application of pXRF measurements as a regional chemostratigraphic correlation tool. The pXRF elemental profiles (e.g., Ca, Fe, Sr, Mn) of the new Morello section and the well-studied Gubbio sections can easily be correlated. This correlation was verified with classic stratigraphic applications such as biostratigraphy and magnetostratigraphy. Furthermore, the first bulk carbonate Campanian to Ypresian $^{87}Sr/^{86}Sr$ record from the Gubbio sections provides a chemostratigraphic reference for the Umbria-March basin. The Morello section seems to have been less altered by burial diagenesis than the classical Gubbio sections and is put forward as an alternative location for sampling the interval around the Cretaceous-Paleogene boundary event. The inclusion of four additional Cretaceous-Paleogene sections from the basin allowed a robust interbasin comparison of the expression of the Cretaceous-Paleogene boundary event in the various proxy records. The major extinction and decrease in productivity from coccolithophorids at the Cretaceous-Paleogene boundary caused a drop in the bulk Sr/Ca ratio across the boundary, while their recovery is expressed as a steady increase in Sr/Ca values. A time interval of ~200 k.y. (66.45–66.25 Ma) that is dominated by an obliquity imprint marks a 2.4 m.y. eccentricity minimum and best fits with the La2011 eccentricity solution. This cyclostratigraphic interpretation also suggests that the first Paleogene hyperthermal event, the Dan-C2, has a similar astronomical configuration as the Paleocene-Eocene thermal maximum (short eccentricity maximum after a 2.4 m.y. eccentricity minimum). This is further evidence for the hypothesis that the Paleogene hyperthermals were astronomically paced.

ACKNOWLEDGMENTS

This research was supported by the Association “Le Montagne di San Francesco” in Coldigioco, Italy. Matthias Sinnesael thanks the Research Foundation of Flanders (FWO) for the awarded Ph.D. fellowship (FWOTM782). Christophe Snoeck was supported by a FWO postdoctoral fellowship. Niels J. de Winter was funded by an awarded Agentschap voor Innovatie door Wetenschap en Technologie (IWT) Ph.D. Flanders fellowship (IWT700-SB-141047). Philippe Claeys thanks the FWO-Hercules foundation for financing the X-ray fluorescence analytical platform at the Vrije Universiteit Brussel, and Vrije Universiteit Brussel for strategic research funding. We thank Nicola Swinburne for the strontium isotope work, Stef Vansteenberge for constructive comments, and Jan Smit for interesting discussions. Any use of trade, firm, or product names is for descriptive purposes only and does not imply endorsement by the U.S. government.

REFERENCES CITED

Alvarez, L.W., Alvarez, W., Asaro, F., and Michel, H.V., 1980, Extraterrestrial cause for the Cretaceous-Tertiary extinction: Science, v. 208, no. 4448, p. 1095–1108, https://doi.org/10.1126/science.208.4448.1095.

Alvarez, W., Arthur, M.A., Fischer, A.G., Lowrie, W., Napoleone, G., Premoli Silva, I., and Rogghenten, W.M., 1977, Upper Cretaceous–Paleocene magnetic stratigraphy at Gubbio, Italy: V. Type section for the Late Cretaceous–Paleocene geomagnetic reversal time scale: Geological Society of America Bulletin, v. 88, p. 383–389, https://doi.org/10.1130/0016-7606(1977)88<383:UCMSAG>2.0.CO;2.

Alvarez, W., Colacicchi, R., and Montanari, A., 1985, Synsedimentary slides and bedding formation in Apennines pelagic limestones: Journal of Sedimentary Research, v. 55, p. 720–734, https://doi.org/10.1306/212F87CE-2B24-11D7-8648000102C1865D.

Alzeni, F., Cipriani, N., Malesani, P., Monechi, S., and Radrizzani, C.P., 1981, Geochemistry at the Cretaceous-Tertiary boundary in the Bottaccione section (Italy): Revista Italiana di Paleontologia Stratigrafica, v. 86, p. 845–854.

Archibald, J.D., Clemens, W.A., Padian, K., Rowe, T., Macleod, N., Barrett, P.M., Gale, A., Holroyd, P., Sues, H.-D., and Arens, N.C., 2010, Cretaceous extinctions: Multiple causes: Science, v. 328, no. 5981, p. 973–974, https://doi.org/10.1126/science.328.5981.973-a.

Arthur, M.A., and Fischer, A., 1977, Upper Cretaceous–Paleocene magnetic stratigraphy at Gubbio, Italy. I. Lithostratigraphy and sedimentology: Geological Society of America Bulletin, v. 88, p. 367–371, https://doi.org/10.1130/0016-7606(1977)88<367:UCMSAG>2.0.CO;2.

Barnet, J.S.K., Littler, K., Kroon, D., Leng, M.J., Westerhold, T., Röhl, U., and Zachos, J.C., 2017, A new high-resolution chronology for the late Maastrichtian warming event: Establishing robust temporal links with the onset of Deccan volcanism: Geology, v. 46, p. 147–150, https://doi.org/10.1130/G39771.1.

Batenburg, S.J., Sprovieri, M., Gale, A.S., Hilgen, F.J., Hüsing, S., Laskar, J., Liebrand, D., Lirer, F., Orue-Etxebarria, X., Pelosi, N., and Smit, J., 2012, Cyclostratigraphy and astronomical tuning of the late Maastrichtian at Zumaia (Basque country, northern Spain): Earth and Planetary Science Letters, v. 359–360, p. 264–278, https://doi.org/10.1016/j.epsl.2012.09.054.

Batenburg, S.J., Gale, A.S., Sprovieri, M., Hilgen, F.J., Thibault, N., Boussaha, M., and Orue-Etxebarria, X., 2014, An astronomical time scale for the Maastrichtian based on the Zumaia and Sopelana sections (Basque country, northern Spain): Journal of the Geological Society, v. 171, p. 165–180, https://doi.org/10.1144/jgs2013-015.

Berger, A., Loutre, M.F., and Laskar, J., 1992, Stability of the astronomical frequencies over the Earth’s history for paleoclimate studies: Science, v. 255, no. 5044, p. 560–566, https://doi.org/10.1126/science.255.5044.560.

Bernaola, G., and Monechi, S., 2007, Calcareous nannofossil extinction and survivorship across the Cretaceous-Paleogene boundary at Walvis Ridge (ODP Hole 1262C, South Atlantic Ocean): Palaeogeography, Palaeoclimatology, Palaeoecology, v. 255, p. 132–156, https://doi.org/10.1016/j.palaeo.2007.02.045.

Bice, D., Montanari, A., and Rusciadelli, G., 2007, Earthquake-induced turbidites triggered by seal level oscillations in the Upper Cretaceous and Paleocene of Italy: Terra Nova, v. 19, p. 387–392, https://doi.org/10.1111/j.1365-3121.2007.00752.x.

Bice, D., Montanari, A., Vucetić, V., and Vucetić, M., 2012, The influence of regional and global climatic oscillations on Croatian climate: International Journal of Climatology, v. 32, p. 1537–1557, https://doi.org/10.1002/joc.2372.

Byrnes, J.S., and Karlstrom, L., 2018, Anomalous K-Pg–aged seafloor attributed to impact-induced mid-ocean ridge magmatism: Science Advances, v. 4, no. 2, eaao2994, https://doi.org/10.1126/sciadv.aao2994.

Chenet, A.-L., Quidelleur, X., Fluteau, F., Courtillot, V., and Bajpai, S., 2007, ^{40}K-^{40}Ar dating of the Main Deccan large igneous province: Further evidence of KTB age and short duration: Earth and Planetary Science Letters, v. 263, p. 1–15, https://doi.org/10.1016/j.epsl.2007.07.011.

Claeys, P.H., Kiessling, W., and Alvarez, W., 2002, Distribution of Chicxulub ejecta at the Cretaceous-Tertiary boundary, *in* Koeberl, C., and MacLeod, K.G., eds., Catastrophic Events and Mass Extinctions: Impacts and Beyond: Geological Society of America Special Paper 356, p. 55–68, https://doi.org/10.1130/0-8137-2356-6.55.

Cleaveland, L.C., Jensen, J., Goese, S., Bice, D.M., and Montanari, A., 2002, Cyclostratigraphic analysis of pelagic carbonates at Monte dei Corvi (Ancona, Italy) and astronomical correlation of the Serravalian-Tortonian boundary: Geology, v. 30, p. 931–934, https://doi.org/10.1130/0091-7613(2002)030<0931:CAOPCA>2.0.CO;2.

Coccioni, R., and Premoli Silva, I., 2015, Revised Upper Albian–Maastrichtian calcareous plankton biostratigraphy and magneto-stratigraphy of the classical Tethyan Gubbio section (Italy): Newsletters on Stratigraphy, v. 48, p. 47–90, https://doi.org/10.1127/nos/2015/0055.

Coccioni, R., Frontalini, F., Bancalà, G., Fornaciari, E., Jovane, L., and Sprovieri, M., 2010, The Dan-C2 hyperthermal event at Gubbio (Italy): Global implications, environmental effects, and cause(s): Earth and Planetary Science Letters, v. 297, p. 298–305, https://doi.org/10.1016/j.epsl.2010.06.031.

Coccioni, R., Bancalà, G., Catanzarit, R., Fornaciari, E., Frontalini, F., Giusberti, L., Jovane, L., Luciani, V., Savian, J., and Sprovieri, M., 2012, An integrated stratigraphic record of the Palaeocene–Lower Eocene at Gubbio (Italy): New insights into the early Palaeogene hyperthermals and carbon isotope excursions: Terra Nova, v. 24, p. 380–386, https://doi.org/10.1111/j.1365-3121.2012.01076.x.

Coccioni, R., Sideri, M., Bancala, G., Catanzariti, R., Frontalini, F., Jovane, L., Montanari, A., and Savain, J., 2013, Integrated stratigraphy (magneto-, bio- and chronostratigraphy) and geochronology of the Palaeogene pelagic succession of the Umbria-Marche Basin (central Italy), *in* Jovane, L., Herrero-Bervera, E., Hinnov, L.A., and Housen, B.A., eds., Magnetic Methods and the Timing of Geological Processes: Geological Society, London, Special Publication 373, p. 111–131, https://doi.org/10.1144/SP373.4.

Cogné, J.P., 2003, PaleoMac: A Macintosh™ application for treating paleomagnetic data and making plate reconstructions: Geochemistry, Geophysics, Geosystems, v. 4, no. 1, 1007, https://doi.org/10.1029/2001GC000227.

Courtillot, V., and Fluteau, F., 2010, Cretaceous extinctions: The volcanic hypothesis: Science, v. 328, no. 5981, p. 973–974, https://doi.org/10.1126/science.328.5981.973-b.

Coxall, H.K., D'Hondt, S., and Zachos, J.C., 2006, Pelagic evolution and environmental recovery after the Cretaceous-Paleogene mass extinction: Geology, v. 34, p. 297–300, https://doi.org/10.1130/G21702.1.

DePaolo, D.J., 2011, Surface kinetic model for isotopic and trace element fractionation during precipitation of calcite from aqueous solution: Geochimica et Cosmochimica Acta, v. 75, p. 1039–1056, https://doi.org/10.1016/j.gca.2010.11.020.

de Winter, N.J., and Claeys, P., 2017, Micro X-ray fluorescence (μXRF) line scanning on Cretaceous rudist bivalves: A new method for reproducible trace element profiles in bivalve calcite: Sedimentology, v. 64, p. 231–251, https://doi.org/10.1111/sed.12299.

de Winter, N.J., Sinnesael, M., Makarona, C., Vansteenberge, S., and Claeys, P., 2017a, Trace element analyses of carbonates using portable and micro-X-ray fluorescence: Performance and optimization of measurement parameters and strategies: Journal of Analytical Atomic Spectrometry, v. 32, p. 1211–1223, https://doi.org/10.1039/C6JA00361C.

de Winter, N.J., Goderis, S., Dehairs, F., Jagt, J.W.M., Fraaije, R.H.B., Van Malderen, S.J.M., Vanhaecke, F., and Claeys, P., 2017b, Tropical seasonality in the late Campanian (Late Cretaceous): Comparison between multiproxy records from three bivalve taxa from Oman: Palaeogeography, Palaeoclimatology, Palaeoecology, v. 485, p. 740–760, https://doi.org/10.1016/j.palaeo.2017.07.031.

D'Hondt, S., Donaghay, P., Zachos, J.C., Luttenberg, D., and Lindinger, M., 1998, Organic carbon fluxes and ecological recovery from the Cretaceous-Tertiary mass extinction: Science, v. 282, no. 5387, p. 276–279, https://doi.org/10.1126/science.282.5387.276.

Dickens, G.R., O'Neil, J.R., Rea, D.K., and Owen, R.M., 1995, Dissociation of oceanic methane hydrate as a cause of the carbon isotope excursion at the end of the Paleocene: Paleoceanography, v. 10, no. 6, p. 965–971, https://doi.org/10.1029/95PA02087.

Dinarès-Turell, J., Westerhold, T., Pujalte, V., Röhl, U., and Kroon, D., 2014, Astronomical calibration of the Danian Stage (early Paleocene) revisited: Settling chronologies of sedimentary records across the Atlantic and Pacific Oceans: Earth and Planetary Science Letters, v. 405, p. 119–131, https://doi.org/10.1016/j.epsl.2014.08.027.

Font, E., Nédélec, A., Ellwood, B.B., Mirão, J., and Silva, P.F., 2011, A new sedimentary benchmark for the Deccan Traps volcanism?: Geophysical Research Letters, v. 38, L24309, https://doi.org/10.1029/2011GL049824.

Font, E., Adatte, T., Sial, A.N., Drude de Lacerda, L., Keller, G., and Punekar, J., 2016, Mercury anomaly, Deccan volcanism, and the end-Cretaceous mass extinction: Geology, v. 44, p. 171–174, https://doi.org/10.1130/G37451.1.

Font, E., Adatte, T., Andrade, M., Keller, G., Mbabi Bitchong, A., Carvallo, C., Ferreira, J., Diogo, Z., and Mirão, J., 2018, Deccan volcanism induced high-stress environment during the Cretaceous-Paleogene transition at Zumaia, Spain: Evidence from magnetic, mineralogical and biostratigraphic records: Earth and Planetary Science Letters, v. 484, p. 53–66, https://doi.org/10.1016/j.epsl.2017.11.055.

Fornaciari, E., Giusberti, L., Luciani, V., Tateo, F., Agnini, C., Backman, J., Oddone, M., and Rio, D., 2007, An expanded Cretaceous-Tertiary transition in a pelagic setting of the southern Alps (central-western Tethys): Palaeogeography, Palaeoclimatology, Palaeoecology, v. 255, p. 98–131, https://doi.org/10.1016/j.palaeo.2007.02.044.

Galeotti, S., Krishnan, S., Pagani, M., Lanci, L., Gaudio, A., Zachos, J.C., Monechi, S., Morelli, G., and Lourens, L., 2010, Orbital chronology of early Eocene hyperthermals from the Contessa Road section, central Italy: Earth and Planetary Science Letters, v. 290, p. 192–200, https://doi.org/10.1016/j.epsl.2009.12.021.

Galeotti, S., Moretti, M., Cappelli, C., Phillips, J., Lanci, L., Littler, K., Monechi, S., Petrizzo, M.R., Premoli Silva, I., and Zachos, J.C., 2015, The Bottaccione section at Gubbio, central Italy: A classical Paleocene Tethyan setting revisited: Newsletters on Stratigraphy, v. 48, p. 325–339, https://doi.org/10.1127/nos/2015/0067.

Gardin, S., and Monechi, S., 1998, Palaeoecological change in the middle to low latitude calcareous nannoplankton at the Cretaceous/Tertiary boundary: Bulletin de la Société Géologique de France, v. 169, no. 5, p. 709–723.

Gardin, S., Galbrun, B., Thibault, N., Coccioni, R., and Premoli Silva, I., 2012, Bio-magnetostratigraphy for the Upper Campanian–Maastrichtian from the Gubbio area, Italy: New results from the Contessa Highway and Bottaccione sections: Newsletters on Stratigraphy, v. 45, p. 75–103, https://doi.org/10.1127/0078-0421/2012/0014.

Gilmour, I., Gilmour, M., Jolley, D., Kelley, S., Kemp, D., Daly, R., and Watson, J., 2013, A high-resolution nonmarine record of an early Danian hyperthermal event, Boltysh crater, Ukraine: Geology, v. 41, p. 783–786, https://doi.org/10.1130/G34292.1.

Gilmour, I., Jolley, D.W., Kemp, D.B., Kelley, S.P., Gilmour, M., Daly, R., Widdowson, M., Keller, G., and Kerr, A.C., 2014, The early Danian hyperthermal event at Boltysh (Ukraine): Relation to Cretaceous-Paleogene boundary events, *in* Keller, G., and Kerr, A.C., eds., Volcanism, Impacts and Mass Extinctions: Causes and Effects: Geological Society of America Special Paper 505, p. 133–146, https://doi.org/10.1130/2014.2505(06).

Hildebrand, A.R., Penfield, G.T., Kring, D.A., Pilkington, M., Camargo, A., Jacobsen, S.B., and Boynton, W.V., 1991, Chicxulub crater: A possible Cretaceous/Tertiary boundary impact crater on the Yucatan Peninsula,

Mexico: Geology, v. 19, p. 867–871, https://doi.org/10.1130/0091-7613(1991)019<0867:CCAPCT>2.3.CO;2.

Hilgen, F.J., Abels, H.A., Kuiper, K.F., Lourens, L.J., and Wolthers, M., 2015, Towards a stable astronomical time scale for the Paleocene: Aligning Shatsky Rise with the Zumaia–Walvis Ridge ODP Site 1262 composite: Newsletters on Stratigraphy, v. 48, p. 91–110, https://doi.org/10.1127/nos/2014/0054.

Hull, P.M., Norris, R.D., Bralower, T.J., and Schueth, J.D., 2011, A role for chance in marine recovery from the end-Cretaceous extinction: Nature Geoscience, v. 4, p. 856–860, https://doi.org/10.1038/ngeo1302.

Husson, D., Galbrun, B., Gardin, S., and Thibault, N., 2014, Tempo and duration of short-term environmental perturbations across the Cretaceous-Paleogene boundary: Stratigraphy, v. 11, p. 159–171.

Jiang, S., Bralower, T.J., Patzkowsky, M.E., Kump, L.R., and Schueth, J.D., 2010, Geographic controls on nannoplankton extinction across the Cretaceous/Palaeogene boundary: Nature Geoscience, v. 3, p. 280–285, https://doi.org/10.1038/ngeo775.

Johnsson, M.J., and Reynolds, R.C., 1986, Clay mineralogy of shale-limestone rhythmites in the Scaglia Rossa (Turonian-Eocene), Italian Apennines: Journal of Sedimentary Petrology, v. 56, p. 501–509.

Jolley, D.W., Daly, R.J., Ebinghaus, A., Kemp, D.B., Gilmour, I., Mac Niocaill, C., and Kelley, S.P., 2017, Centennial to decadal vegetation community changes linked to orbital and solar forcing during the Dan-C2 hyperthermal event: Journal of the Geological Society, v. 174, p. 1019–1030, https://doi.org/10.1144/jgs2017-022.

Kaiho, K., Kajiwara, Y., Tazaki, K., Ueshima, M., Takeda, N., Kawahata, H., Arinobu, T., Ishiwatari, R., Hirai, A., and Lamolda, M.A., 1999, Oceanic primary productivity and dissolved oxygen levels at the Cretaceous/Tertiary boundary: Their decrease, subsequent warming, and recovery: Paleoceanography, v. 14, p. 511–524, https://doi.org/10.1029/1999PA900022.

Kavalieris, I., Khashgerel, B.-E., Morgan, L.E., Undrakhtamir, A., and Borohul, A., 2017, Characteristics and $^{40}Ar/^{39}Ar$ geochronology of the Erdenet Cu-Mo deposit, Mongolia: Economic Geology and the Bulletin of the Society of Economic Geologists, v. 112, p. 1033–1054, https://doi.org/10.5382/econgeo.2017.4500.

Keller, G., Adatte, T., Pardo, A., Bajpai, S., Khosla, A., and Samant, B., 2010, Cretaceous extinctions: Evidence overlooked: Science, v. 328, no. 5981, p. 974–975, https://doi.org/10.1126/science.328.5981.974-a.

Keller, G., Mateo, P., Punekar, J., Khozyem, H., Gertsch, B., Spangenberg, J., Bitchong, A.M., and Adatte, T., 2018, Environmental changes during the Cretaceous-Paleogene mass extinction and Paleocene-Eocene thermal maximum: Implications for the Anthropocene: Gondwana Research, v. 56, p. 69–89, https://doi.org/10.1016/j.gr.2017.12.002.

Kennett, J.P., and Stott, L.D., 1991, Abrupt deep-sea warming, palaeoceanographic changes and benthic extinctions at the end of the Palaeocene: Nature, v. 353, p. 225–229, https://doi.org/10.1038/353225a0.

Kirschvink, J.L., 1980, The least-squares line and plane and the analysis of palaeomagnetic data: Geophysical Journal International, v. 62, p. 699–718, https://doi.org/10.1111/j.1365-246X.1980.tb02601.x.

Laskar, J., Fienga, A., Gastineau, M., and Manche, H., 2011a, La2010: A new orbital solution for the long-term motion of the Earth: Astronomy & Astrophysics, v. 532, no. A89, 15 p., https://doi.org/10.1051/0004-6361/201116836.

Laskar, J., Gastineau, M., Delisle, J.-B., Farrés, A., and Fienga, A., 2011b, Strong chaos induced by close encounters with Ceres and Vesta: Astronomy & Astrophysics, v. 532, p. L4, https://doi.org/10.1051/0004-6361/201117504.

Lauretano, V., Littler, K., Polling, M., Zachos, J.C., and Lourens, L.J., 2015, Frequency, magnitude and character of hyperthermal events at the onset of the early Eocene climatic optimum: Climate of the Past, v. 11, p. 1313–1324, https://doi.org/10.5194/cp-11-1313-2015.

Laurin, J., Meyers, S.R., Galeotti, S., and Lanci, L., 2016, Frequency modulation reveals the phasing of orbital eccentricity during Cretaceous oceanic anoxic event II and the Eocene hyperthermals: Earth and Planetary Science Letters, v. 442, p. 143–156, https://doi.org/10.1016/j.epsl.2016.02.047.

Le Callonec, L., Renard, M., De Rafélis, M., Minoletti, F., Beltran, C., and Du Chêne, R.J., 2014, Evolution of trace element contents (Sr and Mn) of hemipelagic carbonates from the Zumaia Paleocene section (Gipuzkoa, Spain): Implications for the knowledge of seawater chemistry during the Selandian: Bulletin de la Société Géologique de France, v. 185, p. 413–435, https://doi.org/10.2113/gssgfbull.185.6.413.

Li, L., and Keller, G., 1998, Abrupt deep-sea warming at the end of the Cretaceous: Geology, v. 26, no. 11, p. 995–998, https://doi.org/10.1130/0091-7613(1998)026<0995:ADSWAT>2.3.CO;2.

Lirer, F., 2000, A new technique for retrieving calcareous microfossils from lithified lime deposits: Micropaleontology, v. 46, no. 4, p. 365–369.

Littler, K., Röhl, U., Westerhold, T., and Zachos, J.C., 2014, A high-resolution benthic stable-isotope record for the South Atlantic: Implications for orbital-scale changes in Late Paleocene–Early Eocene climate and carbon cycling: Earth and Planetary Science Letters, v. 401, p. 18–30, https://doi.org/10.1016/j.epsl.2014.05.054.

Lourens, L., Sluijs, A., Kroon, D., Zachos, J.C., Thomas, E., Röhl, U., Bowles, J., and Raffi, I., 2005, Astronomical pacing of late Palaeocene to early Eocene global warming events: Nature, v. 435, p. 1083–1087, https://doi.org/10.1038/nature03814.

Lowrie, W., Alvarez, W., Napoleone, G., Perch-Nielsen, K., Premoli Silva, I., and Toumarkine, M., 1982, Paleogene magnetic stratigraphy in Umbrian pelagic carbonate rocks: The Contessa sections, Gubbio: Geological Society of America Bulletin, v. 93, p. 414–432, https://doi.org/10.1130/0016-7606(1982)93<414:PMSIUP>2.0.CO;2.

Lowrie, W., Alvarez, W., and Asaro, F., 1990, The origin of the White Beds below the Cretaceous-Tertiary boundary in the Gubbio section, Italy: Earth and Planetary Science Letters, v. 98, p. 303–312, https://doi.org/10.1016/0012-821X(90)90032-S.

Luterbacher, H.P., and Premoli Silva, I., 1964, Biostratigrafi a del limite creteceo-terziario nell'Appennino central: Rivista Italiana di Paleontologia e Stratigrafia, v. 70, p. 67–128.

Margolis, S.V., Mount, J.F., Doehne, E., Showers, W., and Ward, P., 1987, The Cretaceous/Tertiary boundary carbon and oxygen isotope stratigraphy, diagenesis, and paleoceanography at Zumaya, Spain: Paleoceanography, v. 2, no. 4, p. 361–377, https://doi.org/10.1029/PA002i004p00361.

McArthur, J.M., Thirlwall, M.F., Gale, A.S., Kennedy, W.J., Burnett, J.A., Mattey, D., and Lord, A.R., 1993, Strontium isotope stratigraphy for the Late Cretaceous: A new curve, based on the English Chalk, *in* Hailwood, E.A., and Kid, R.B., eds., High Resolution Stratigraphy: Geological Society, London, Special Publication 70, p. 195–209, https://doi.org/10.1144/GSL.SP.1993.070.01.14.

McArthur, J.M., Howarth, R.J., and Shields, G.A., 2012, Strontium isotope stratigraphy, *in* Gradstein, F., Ogg, J., Schmitz, M., and Ogg, G., eds., The Geological Time Scale 2012: Amsterdam, Elsevier, p. 127–144, https://doi.org/10.1016/B978-0-444-59425-9.00007-X.

McFadden, P.L., and McElhinny, M.W., 1990, Classification of the reversal test in palaeomagnetism: Geophysical Journal International, v. 103, p. 725–729, https://doi.org/10.1111/j.1365-246X.1990.tb05683.x.

Montanari, A., 1986, Spherules from the Cretaceous/Tertiary boundary clay at Gubbio, Italy: The problem of outcrop contamination: Geology, v. 14, p. 1024–1026, https://doi.org/10.1130/0091-7613(1986)14<1024:SFTCBC>2.0.CO;2.

Montanari, A., 1991, Authigenesis of impact spheroids in the K/T boundary clay from Italy: New constraints for high-resolution stratigraphy of terminal Cretaceous events: Journal of Sedimentary Petrology, v. 61, no. 3, p. 315–339, https://doi.org/10.1306/D42676FE-2B26-11D7-8648000102C1865D.

Montanari, A., and Koeberl, C., 2000, Impact Stratigraphy: The Italian Record: Heidelberg, Germany, Springer, 364 p.

Montanari, A., Hay, R.L., Alvarez, W., Asaro, F., Michel, H.V., Alvarez, L.W., and Smit, J., 1983, Spheroids at the Cretaceous-Tertiary boundary are altered impact droplets of basaltic composition: Geology, v. 11, p. 668–671, https://doi.org/10.1130/0091-7613(1983)11<668:SATCBA>2.0.CO;2.

Montanari, A., Chan, L.S., and Alvarez, W., 1989, Synsedimentary tectonics in the Late Cretaceous–Early Tertiary pelagic basin of the Northern Apennines, *in* Crevello, P., Wilson, J.L., Sarg, R., and Reed, F., eds., Controls on Carbonate Platforms and Basin Development: Society of Economic Paleontologists and Mineralogists (SEPM) Special Publication 44, p. 379–399, https://doi.org/10.2110/pec.89.44.0379.

Montanari, A., Farley, K., Claeys, P., De Vleeschouwer, D., de Winter, N., Vansteenberge, S., Sinnesael, M., and Koeberl, C., 2017, Stratigraphic record of the asteroidal Veritas breakup in the Tortonian Monte dei Corvi section (Ancona, Italy): Geological Society of America Bulletin, v. 129, p. 1357–1376, https://doi.org/10.1130/B31476.1.

Mukhopadhyay, S., Farley, K.A., and Montanari, A., 2001, A short duration of the Cretaceous-Tertiary boundary event: Evidence from extraterrestrial

helium-3: Science, v. 291, no. 5510, p. 1952–1955, https://doi.org/10.1126/science.291.5510.1952.

Mukhopadhyay, S.K., Pal, S., and Shrivastava, J.P., 2017, Comments on the paper published by Sial et al. (2016), "Mercury enrichments and Hg isotopes in Cretaceous-Paleogene boundary successions: Links to volcanism and palaeoenvironmental impacts" (Cretaceous Research, v. 66, pp. 60–81): Cretaceous Research, v. 76, p. 81–83, https://doi.org/10.1016/j.cretres.2016.12.006.

Muller, R.A., and MacDonald, G.J., 2000, Ice Ages and Astronomical Causes: Data, Spectral Analysis and Mechanisms: London, Springer, 318 p.

Odin, G.S., Hurford, A.J., and Montanari, A., 1992, Study of a presumably volcano-sedimentary layer near the Cretaceous-Paleogene boundary in the Central Apennines (Italy), *in* Odin, G.S., ed., Phanerozoic Time Scale: International Union of Geological Sciences Subcommission on Geochronology Bulletin de Liaison 11, p. 26–28.

Paine, J.H., Nomade, S., and Renne, P.R., 2006, Quantification of ^{39}Ar recoil ejection from GA1550 biotite during neutron irradiation as a function of grain dimensions: Geochimica et Cosmochimica Acta, v. 70, p. 1507–1517, https://doi.org/10.1016/j.gca.2005.11.012.

Percival, L.M.E., Jenkyns, H.C., Mather, T.A., Dickson, A.J., Batenburg, S.J., Ruhl, M., Hesselbo, S.P., Barclay, R., Jarvis, I., Robinson, S.A., and Woelders, L., 2018, Does large igneous province volcanism always perturb the mercury cycle? Comparing the records of oceanic anoxic event 2 and the end-Cretaceous to other Mesozoic events: American Journal of Science, v. 318, no. 8, p. 799–860, https://doi.org/10.2475/08.2018.01.

Quillévéré, F., Norris, R.D., Kroon, D., and Wilson, P.A., 2008, Transient ocean warming and shifts in carbon reservoirs during the early Danian: Earth and Planetary Science Letters, v. 265, p. 600–615, https://doi.org/10.1016/j.epsl.2007.10.040.

Raup, D.M., and Sepkoski, J.J., 1982, Mass extinctions in the marine fossil record: Science, v. 215, no. 4539, p. 1501–1503, https://doi.org/10.1126/science.215.4539.1501.

Ravizza, G., and Peucker-Ehrenbrink, B., 2003, Chemostratigraphic evidence of Deccan volcanism from the marine isotope record: Science, v. 302, no. 5649, p. 1392–1395, https://doi.org/10.1126/science.1089209.

Ravizza, G., and VonderHaar, D., 2012, A geochemical clock in earliest Paleogene pelagic carbonates based on the impact-induced Os isotope excursion at the Cretaceous-Paleogene boundary: Paleoceanography, v. 27, PA3219, https://doi.org/10.1029/2012PA002301.

Renard, M., 1986, Pelagic carbonate chemostratigraphy (Sr, Mg, ^{18}O, ^{13}C): Marine Micropaleontology, v. 10, p. 117–164, https://doi.org/10.1016/0377-8398(86)90027-7.

Renard, M., Delacotte, O., and Letolle, R., 1982, Le strontium et les isotopes stables dans les carbonates totaux de quelques sites de l'Atlantique et de la Tethys: Bulletin de la Société Géologique de France, ser. 7, v. 24, no. 3, p. 519–534, https://doi.org/10.2113/gssgfbull.S7-XXIV.3.519.

Renne, P.R., Balco, G., Ludwig, K.R., Mundil, R., and Min, K., 2011, Response to the comment by W.H. Schwarz et al. on "Joint determination of ^{40}K decay constants and ^{40}Ar/^{40}K for the Fish Canyon sanidine standard, and improved accuracy for ^{40}Ar/^{39}Ar geochronology" by P.R. Renne et al. (2010): Geochimica et Cosmochimica Acta, v. 75, p. 5097–5100, https://doi.org/10.1016/j.gca.2011.06.021.

Renne, P.R., Deino, A.L., Hilgen, F.J., Kuiper, K.F., Mark, D.F., Mitchell, W.S., III, Morgan, L.E., Mundil, R., and Smit, J., 2013, Time scales of critical events around the Cretaceous-Paleogene boundary: Science, v. 339, no. 6120, p. 684–687, https://doi.org/10.1126/science.1230492.

Renne, P.R., Sprain, C.J., Richards, M.A., Self, S., Vanderkluysen, L., and Pande, K., 2015, State shift in Deccan volcanism at the Cretaceous-Paleogene boundary, possibly induced by impact: Science, v. 350, no. 6256, p. 76–78, https://doi.org/10.1126/science.aac7549.

Richards, M.A., Alvarez, W., Self, S., Karlstrom, L., Renne, P.R., Manga, M., Sprain, C.J., Smit, J., Vanderkluysen, L., and Gibson, S.A., 2015, Triggering of the largest Deccan eruptions by the Chicxulub impact: Geological Society of America Bulletin, v. 127, p. 1507–1520, https://doi.org/10.1130/B31167.1.

Rickaby, R.E.M., Schrag, D.P., Zondervan, I., and Riebesell, U., 2002, Growth rate dependence of Sr incorporation during calcification of *Emiliania huxleyi*: Global Biogeochemical Cycles, v. 16, no. 1, 1006, https://doi.org/10.1029/2001GB001408.

Robinson, N., Ravizza, G., Coccioni, R., Peucker-Ehrenbrink, B., and Norris, R., 2009, A high-resolution marine ^{187}Os/^{188}Os record for the late Maastrichtian: Distinguishing the chemical fingerprints of Deccan volcanism and the KP impact event: Earth and Planetary Science Letters, v. 281, p. 159–168, https://doi.org/10.1016/j.epsl.2009.02.019.

Roggenthen, W.M., and Napoleone, G., 1977, Upper Cretaceous–Paleocene magnetic stratigraphy at Gubbio, Italy. IV. Upper Maastrichtian–Paleocene magnetic stratigraphy: Geological Society of America Bulletin, v. 88, p. 378–382, https://doi.org/10.1130/0016-7606(1977)88<378:UCMSAG>2.0.CO;2.

Schoene, B., Samperton, K.M., Eddy, M.P., Keller, G., Adatte, T., Bowring, S.A., Khadri, S.F.R., and Gertch, B., 2015, U-Pb geochronology of the Deccan Traps and relation to the end-Cretaceous mass extinction: Science, v. 347, no. 6218, p. 182–184, https://doi.org/10.1126/science.aaa0118.

Schulte, P., Speijer, R., Mai, H., and Kontny, A., 2006, The Cretaceous-Paleogene (K-P) boundary at Brazos, Texas: Sequence stratigraphy, depositional events and the Chicxulub impact: Sedimentary Geology, v. 184, p. 77–109, https://doi.org/10.1016/j.sedgeo.2005.09.021.

Schulte, P., and 40 others, 2010, The Chicxulub asteroid impact and mass extinction at the Cretaceous-Paleogene boundary: Science, v. 327, no. 5970, p. 1214–1218, https://doi.org/10.1126/science.1177265.

Sial, A.N., Chen, J., Lacerda, L.D., Frei, R., Tewari, V.C., Pandit, M.K., Gaucher, C., Ferreira, V.P., Cirilli, S., Peralta, S., Korte, C., Barbosa, J.A., and Pereira, N.S., 2016, Mercury enrichment and Hg isotopes in Cretaceous-Paleogene boundary successions: Links to volcanism and palaeoenvironmental impacts: Cretaceous Research, v. 66, p. 60–81, https://doi.org/10.1016/j.cretres.2016.05.006.

Sinnesael, M., De Vleeschouwer, D., Coccioni, R., Claeys, P., Frontalini, F., Jovane, L., Savian, J.F., and Montanari, A., 2016a, High-resolution multiproxy cyclostratigraphic analysis of environmental and climatic events across the Cretaceous-Paleogene boundary in the classic pelagic succession of Gubbio (Italy), *in* Menichetti, M., Coccioni, R., and Montanari, A., eds., The Stratigraphic Record of Gubbio: Integrated Stratigraphy of the Late Cretaceous–Paleogene Umbria-Marche Pelagic Basin: Geological Society of America Special Paper 524, p. 115–137, https://doi.org/10.1130/2016.2524(09).

Sinnesael, M., Zivanovic, M., De Vleeschouwer, D., Claeys, P., and Schoukens, J., 2016b, Astronomical component estimation (ACE v.1) by time-variant sinusoidal modeling: Geoscientific Model Development, v. 9, p. 3517–3531, https://doi.org/10.5194/gmd-9-3517-2016.

Sinnesael, M., de Winter, N.J., Snoeck, C., Montanari, A., and Claeys, P., 2018, An integrated pelagic carbonate multi-proxy study using portable X-ray fluorescence (pXRF): Maastrichtian strata from the Bottaccione Gorge, Gubbio, Italy: Cretaceous Research, v. 91, p. 20–32, https://doi.org/10.1016/j.cretres.2018.04.010.

Sluijs, A., Brinkhuis, H., Schouten, S., Bohaty, S.M., John, C.M., Zachos, J.C., Reichart, G.-J., Sinninghe Damsté, J.S., Crouch, E.M., and Dickens, G.R., 2007, Environmental precursors to rapid light carbon injection at the Palaeocene/Eocene boundary: Nature, v. 450, p. 1218–1221, https://doi.org/10.1038/nature06400.

Smit, J., 1982, Extinction and evolution of planktonic foraminifera after a major impact at the Cretaceous/Tertiary boundary, *in* Silver, L.T., and Schultz, P.H., eds., Geological Implications of Impacts of Large Asteroids and Comets on the Earth: Geological Society of America Special Paper 190, p. 329–352, https://doi.org/10.1130/SPE190-p329.

Smit, J., and Hertogen, J., 1980, An extraterrestrial event at the Cretaceous-Tertiary boundary: Nature, v. 285, p. 198–200, https://doi.org/10.1038/285198a0.

Smit, J., and ten Kate, W., 1982, Trace-element patterns at the Cretaceous-Tertiary boundary: Consequences of a large impact: Cretaceous Research, v. 3, p. 307–332, https://doi.org/10.1016/0195-6671(82)90031-3.

Smit, J., Koeberl, C., Claeys, P., and Montanari, A., 2016, Mercury anomaly, Deccan volcanism, and the end-Cretaceous mass extinction: Geology, v. 44, p. e381, https://doi.org/10.1130/G37683C.1.

Sprain, C.J., Renne, P.R., Clemens, W.A., and Wilson, G.P., 2018, Calibration of chron C29r: New high-precision geochronologic and paleomagnetic constraints from the Hell Creek region, Montana: Geological Society of America Bulletin, v. 130, p. 1615–1644, https://doi.org/10.1130/B31890.1.

Stap, L., Lourens, L.J., Thomas, E., Sluijs, A., Bohaty, S., and Zachos, J.C., 2010, High-resolution deep-sea carbon and oxygen isotope records of Eocene thermal maximum 2 and H2: Geology, v. 38, p. 607–610, https://doi.org/10.1130/G30777.1.

Stoll, H.M., and Schrag, D.P., 2000, Coccolith Sr/Ca as a new indicator of coccolithophorid calcification and growth rate: Geochemistry Geophysics Geosystems, v. 1, no. 1, p. 1006, https://doi.org/10.1029/1999GC000015.

Swisher, C.C., III, Grajales-Nishimura, J.M., Montanari, A., Margolis, S.V., Claeys, P., Alvarez, W., Renne, P., Cedillo-Pardo, E., Maurrasse, F., Curtis, G., Smit, J., and McWilliams, M.O., 1992, Coeval $^{40}Ar/^{39}Ar$ ages of 65.0 million years ago from Chicxulub crater melt rock and Cretaceous-Tertiary boundary tektites: Science, v. 257, no. 5072, p. 954–958, https://doi.org/10.1126/science.257.5072.954.

Thibault, N., Harlou, R., Schovsbo, N.H., Stemmerik, L., and Surlyk, F., 2016a, Late Cretaceous (late Campanian–Maastrichtian) sea-surface temperature record of the Boreal Chalk Sea: Climate of the Past, v. 12, p. 429–438, https://doi.org/10.5194/cp-12-429-2016.

Thibault, N., Galbrun, B., Gardin, S., Minoletti, F., and Le Callonnec, L., 2016b, The end-Cretaceous in the southwestern Tethys (Elles, Tunisia): Orbital calibration of paleoenvironmental events before the mass extinction: International Journal of Earth Sciences, v. 105, p. 771–795, https://doi.org/10.1007/s00531-015-1192-0.

Wade, B.S., Pearson, P.N., Berggren, W.A., and Pälike, H., 2011, Review and revision of Cenozoic tropical planktonic foraminiferal biostratigraphy and calibration to the geomagnetic polarity and astronomical time scale: Earth-Science Reviews, v. 104, p. 111–142, https://doi.org/10.1016/j.earscirev.2010.09.003.

Westerhold, T., Röhl, U., Raffi, I., Fornaciari, E., Monechi, S., Reale, V., Bowles, J., and Evans, H.F., 2008, Astronomical calibration of the Paleocene time: Palaeogeography, Palaeoclimatology, Palaeoecology, v. 257, p. 377–403, https://doi.org/10.1016/j.palaeo.2007.09.016.

Westerhold, T., Röhl, U., Donner, B., McCarren, H.K., and Zachos, J.C., 2011, A complete high-resolution Paleocene benthic stable isotope record for the central Pacific (ODP Site 1209): Paleoceanography, v. 26, PA2216, https://doi.org/10.1029/2010PA002092.

Woelders, L., Vellekoop, J., Weltje, G.J., de Nooijer, L., Reichart, G.J., Peterse, F., Claeys, P., and Speijer, R.P., 2018, Robust multi-proxy data integration, using Late Cretaceous paleotemperature records as a case study: Earth and Planetary Science Letters, v. 500, p. 215–224, https://doi.org/10.1016/j.epsl.2018.08.010.

Zachos, J.C., and Arthur, M.A., 1986, Paleoceanography of the Cretaceous/Tertiary boundary event: Inferences from stable isotopic and other data: Paleoceanography, v. 1, no. 1, p. 5–26, https://doi.org/10.1029/PA001i001p00005.

Zachos, J.C., Pagani, M., Sloan, L., Thomas, E., and Billups, K., 2001, Science, trends, rhythms, and aberrations in global climate, 65 Ma to present: Science, v. 292, p. 686–693, https://doi.org/10.1126/science.1059412.

Zachos, J.C., McCarren, H., Murphy, B., Röhl, U., and Westerhold, T., 2010, Tempo and scale of the late Paleocene and early Eocene carbon isotope cycles: Implications for the origin of hyperthermals: Earth and Planetary Science Letters, v. 299, p. 242–249, https://doi.org/10.1016/j.epsl.2010.09.004.

Zeebe, R.E., Zachos, J.C., and Dickens, G.R., 2009, Carbon dioxide forcing alone insufficient to explain Palaeocene–Eocene thermal maximum warming: Nature Geoscience, v. 2, p. 576–580, https://doi.org/10.1038/ngeo578.

Manuscript Accepted by the Society 18 January 2019
Manuscript Published Online 29 May 2019

Printed in the USA